Report No. ACNP-63002

PATHFINDER ATOMIC POWER PLANT
PRESSURE DROP AND VOID FRACTION EXPERIMENTS IN SIMULATED PATHFINDER BOILER FUEL ELEMENTS

March 8, 1963

Submitted to

U. S. ATOMIC ENERGY COMMISSION
NORTHERN STATES POWER COMPANY
and
CENTRAL UTILITIES ATOMIC POWER ASSOCIATES

by

ALLIS-CHALMERS MANUFACTURING COMPANY
ATOMIC ENERGY DIVISION
Milwaukee 1, Wisconsin

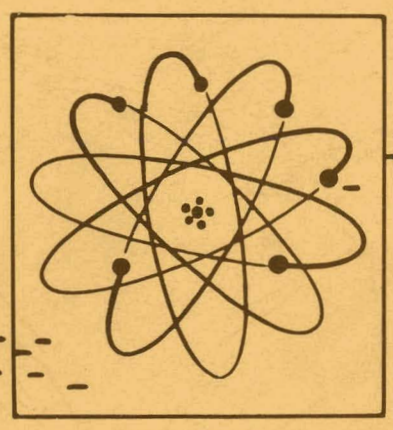

Ref: AEC Contract No. AT(11-1)-589

DISCLAIMER

LEGAL NOTICE

This report was prepared as an account of Government sponsored work. Neither the United States, nor the Commission, nor Allis-Chalmers Manufacturing Company, nor any person acting on behalf of the Commission or Allis-Chalmers Manufacturing Company:

A. Makes any warranty or representation to others, expressed or implied, with respect to the accuracy, completeness, or usefulness of the information contained in this report, or that the use of any information, apparatus, method, or process disclosed in this report may not infringe privately owned rights; or

B. Assumes any liabilities to others with respect to the use of, or for damages resulting from the use of any information, apparatus, method, or process disclosed in this report.

As used in the above, 'person acting on behalf of the Commission or Allis-Chalmers Manufacturing Company' includes any employe or contractor of the Commission, or Allis-Chalmers Manufacturing Company or employe of such contractor, to the extent that such employe or contractor of the Commission, or Allis-Chalmers Manufacturing Company or employe of such contractor prepares, disseminates, or provides access to, any information pursuant to his employment or contract with the Commission or Allis-Chalmers Manufacturing Company or his employment with such contractor.

PRESSURE DROP AND VOID FRACTION EXPERIMENTS IN SIMULATED PATHFINDER BOILER FUEL ELEMENTS

by G. Kangas and K. Neusen

Submitted to

U. S. ATOMIC ENERGY COMMISSION
NORTHERN STATES POWER COMPANY
and
CENTRAL UTILITIES ATOMIC POWER ASSOCIATES

by

ALLIS-CHALMERS MANUFACTURING COMPANY

Under
Agreement dated 2nd Day of May 1957, as Amended
between
Allis-Chalmers Mfg. Co. & Northern States Power Co.
under
AEC Contract No. AT(11-1)-589

March 8, 1963

Classification – UNCLASSIFIED

Reviewed by

Authorized Classifying Official

Approved:

C. B. Graham
Manager
Nuclear Power Dept.-Greendale

ALLIS-CHALMERS MANUFACTURING COMPANY
ATOMIC ENERGY DIVISION
MILWAUKEE 1, WISCONSIN

Approved:

Hibbert Hill
Vice President-
Engineering

NORTHERN STATES POWER COMPANY
15 SOUTH FIFTH STREET
MINNEAPOLIS 2, MINNESOTA

PATHFINDER ATOMIC POWER PLANT

PRESSURE DROP AND VOID FRACTION EXPERIMENTS IN SIMULATED PATHFINDER BOILER FUEL ELEMENTS

Distribution

USAEC, Chicago Operations Office -- 9800 South Cass Avenue, Argonne, Illinois	8
USAEC, Division of Reactor Development -- Washington 25, D. C.	8
USAEC, OTIE -- Oak Ridge, Tennessee . . . Offset Master Plus	20
Northern States Power Company and CUAPA	26
Allis-Chalmers Manufacturing Company	39
	101

FOREWORD

This report "Pressure Drop and Void Fraction Experiments in Simulated Pathfinder Boiler Fuel Elements" is one of a series of reports on research and development in connection with the design of Pathfinder Atomic Power Plant.

The Pathfinder Plant will be located at a site near Sioux Falls, South Dakota, and is scheduled for operation in 1963. Owners and operators of the plant will be the Northern States Power Company of Minneapolis, Minnesota. Allis-Chalmers is performing the research, development, and design as well as being responsible for plant construction.

The U. S. Atomic Energy Commission, through Contract No. AT(11-1)-589 with Northern States Power Company, and Central Utilities Atomic Power Associates (CUAPA) are sponsors of the research and development program.

The plant's reactor will be of the Controlled Ricirculation Boiling Reactor type with Nuclear Superheater.

CONTENTS

	Page
Distribution	ii
Foreword	iii
List of Illustrations	vii
List of Symbols	x
1.0 Introduction	1
2.0 Objective	1
3.0 Conclusion	2
4.0 General Review	3
4.1 Pressure Drops	3
4.2 Void Fraction	5
5.0 Theoretical Considerations	7
5.1 Pressure Drops	7
5.2 Void Fraction	10
6.0 Axial Pressure Profile Downstream From A Spacer, Single Phase Flow Experiment	14
6.1 Equipment	14
6.2 Axial Pressure Profiles	17
6.3 Friction Factors	19
6.4 Form Loss Coefficients	19
6.5 Conclusion	21

CONTENTS (Continued)

Page

7.0 Pressure Profile Downstream Of A Spacer In A Two-Phase Flow Experiment 24

7.1 Equipment 24

7.2 Test Conditions 24

7.3 Pressure Profiles 24

7.4 Loss Coefficients 27

7.5 Friction Factors 27

7.6 Conclusions 30

8.0 Boiling Pressure Drops And Void Fractions In A 4 x 4 Array Experiment 31

8.1 Equipment 31

8.1.1 Heat Transfer Loop 31

8.1.2 Test Section 31

8.1.3 Loop Instrumentation 38

8.1.3.1 Flow Measurement 38

8.1.3.2 System Pressure 38

8.1.3.3 Differential Pressure Drops 38

8.1.3.4 Bulk Temperature Measurements 39

8.1.3.5 Test Section Power 39

8.1.4 Void Fraction Equipment 39

8.2 Void Measuring Procedure 42

8.3 Results 44

8.3.1 Isothermal Pressure Drops 44

CONTENTS (Continued)

Page

8.3.2 Bulk Boiling Frictional Pressure Drops 45

8.3.3 Bulk Boiling Form Pressure Drops 49

8.3.4 Local Boiling Pressure Drops 55

8.3.5 Over-All Pressure Drops 58

8.3.6 Void Fractions 59

8.4 Conclusions 74

9.0 Effect Of Array Size On Boiling Phenomenon 74

9.1 Description Of Test Section 74

9.2 Results And Conclusions 76

10.0 Recommendations 78

11.1 Application Of Results To Pathfinder 78

ILLUSTRATIONS

Figure Number		Page
1.	Low Pressure Loop Schematic Diagram	15
2.	Low Pressure Air-Water Loop	16
3.	Boiler Prototype Element Sample Over-all Pressure Drop	18
4.	Boiler Prototype Element Isothermal Friction Factors	20
5.	Entrance and Exit Form Loss Coefficients	22
6.	Tube Sheet Form Loss Coefficients	23
7.	Sample Pressure Profile for Air-Water Mixture Flowing in an 81 Pin Prototype Element	25
8.	Sample Pressure Profile for Air-Water Mixture Flowing in an 81 Pin Prototype Element	26
9.	Two-Phase Effect on Entrance and Exit Losses	28
10.	Two-Phase Effect on Tube Sheet Losses	29
11.	Two-Phase Multipliers for Air-Water Flow in a Rod Bundle	32
12.	Heat Transfer Loop Schematic Diagram	33
13.	Sixteen Pin Test Section Assembly	35
14.	Cross Section of 16 Pin Test Section	36
15.	Pin Bundle Spacer Arrangement	37
16.	Gamma Attenuation Equipment Block Diagram	40
17.	Boiling Friction Losses as a Function of Quality and Mass Velocity	48
18.	Boiling Effect on Form Loss Coefficient	52

ILLUSTRATIONS (Continued)

Figure Number		Page
19.	Boiling Effect on Form Loss Coefficient	53
20.	Boiling Effect on Form Loss Coefficient	54
21.	Effect of Local Boiling on Friction Factors	57
22.	Local Void Fraction Data Pin Row Centerline to Position Equidistant Between Pin Rows (Data Superimposed 16 Pin Tests-Typical)	61
23.	Local Void Fraction Data Outermost Pin Row Centerline to Position Equidistant Between Pin Rows (Data Superimposed 16 Pin Test-Typical)	62
24.	Local Void Fraction Data Centerline of Outermost Pin Row to Box Wall (Data Superimposed 16 Pin Tests-Typical)	63
25.	Local Void Fraction Distribution (Mean Curves from Superposition Averaging) Pin Row Centerline to Position Equidistant Between Pin Rows (16 Pin Tests)	65
26.	Local Void Fraction Distribution (Mean Curves from Superposition Averaging) Outermost Pin Row Centerline to Position Equidistant Between Pin Rows (16 Pin Tests)	66
27.	Local Void Fraction Distribution (Mean Curves from Superposition Averaging) Centerline of Outermost Pin Row to Box Wall) (16 Pin Tests)	67
28.	Local Void Fraction Distribution Vertical Upflow 600 PSI (16 Pin Tests)	70

ILLUSTRATIONS (Continued)

Figure Number		Page
29.	Gross Region-Wise Void Distributions Vertical Upflow 600 PSI (16 Pin Tests)	72
30.	Over-all Mean Steam-Water Void Fraction ($\overline{Rg}$) 600 PSIA . . .	73
31.	Two-Phase Frictional Pressure Drop Multipliers at 600 PSIA (81 Pin Test Section)	77
32.	Pressure Drop-Flow Curves for Various Boiler Powers	79

LIST OF SYMBOLS

(In Consistent Units)

D_e - equivalent diameter

e - Naperian base

f - Friction factor

g_c - Gravitational constant

G - Mass velocity

h - Heat transfer coefficient

k - Form pressure loss coefficient

L - Section length

N - Radiation intensity (per unit area) at detector

N* - Incident radiation intensity (per unit area)

P - Static pressure (also pitch in square lattice)

ΔP - Static pressure difference

R_g - Void fraction

T - Temperature

v - Specific volume

X - Quality (weight fraction gas flowing) or radiation path length

ΔZ - Change in elevation

Greek

β - Attenuation coefficient

Δ - Difference

ρ - Density

LIST OF SYMBOLS (Continued)

σ - Area ratio (always less than unity; see page 9)

Σ - Constriction area ratio (always less than unity, see page 9)

ϕ - Heat flux

φ_{LO}^2 - Two-phase frictional multiplier

Subscripts

c - Denotes constriction parameter

iso - Isothermal condition (all liquid)

f - Saturated liquid for properties, friction for pressure drop

J&L - Jens & Lottes

L - Liquid

rec - Recoverable

unrec - Unrecoverable

s - Steam

sat - Saturated

TP - Denotes Two-phase

v - Vapor

1.0 INTRODUCTION

A comprehensive heat transfer research and development program has been undertaken in support of the Pathfinder boiling water, integral superheating reactor. To a considerable extent this effort has been directed toward understanding the phenomenon of boiling flow in a parallel rod array.

Despite the rather general application of the parallel rod type fuel element in nuclear reactors, the development of heat transfer and fluid flow technology for this geometry has not received corresponding attention. Rather, the trend has been to treat the parallel rod case as simply as extension of the more thoroughly studied geometries of round tube, parallel plate (and/or rectangular channel), and annulus, generally by means of the equivalent diameter concept. In many cases experimental programs have been restricted to those which can only confirm this "extension" approach. However, the results from these programs have generally been affirmative.

In the present program, attention was directed to those features of the parallel rod flow which either cannot be included in "other geometry" considerations or to which extension of results from other geometries might be questionable. The most important of these, in the case of the Pathfinder fuel element, is the requirement for spacing the rods (mechanically fixing to prevent bowing and/or vibration) which was met by the application of intermittent grid networks within the rod array.

2.0 OBJECTIVE

The experiments described in this report were performed to accomplish the following:

1. Study the effects of tube-sheet type spacers on the axial pressure profile in a simulated fuel element.
2. Measure the effect of boiling on the frictional and spacer type pressure losses in a 6 ft long test section.
3. Measure the void fraction in a test section by a fine gamma ray traversing technique.
4. Determine if experimental data taken from a 4 x 4 array is applicable to a larger array.

3.0 CONCLUSIONS

1. With respect to the development of the flow field downstream from a spacer, the flow quickly becomes established except near the bundle entrance. It is desirable to measure the unestablished, single-phase frictional losses in this region, but conventional two-phase multipliers can be applied. (In Pathfinder, boiling never occurs in this region.)
2. With respect to two-phase pressure losses in boiling flow over a rod array with intermittent spacers, existing relations for single phase friction (3), for two-phase frictional multipliers (8 and 9), for two-phase form loss multipliers (10), and for voids in calculating pressure drop components are applicable (except as noted above in 1).
3. With respect to the void fractions in boiling flow over a rod array, the local radial void distribution is non-uniform with a uniform radial power distribution and the over-all integrated void fractions tend to support the homogeneous model.

4. There was no appreciable effect of array size on single-phase and two-phase friction and form type pressure losses and over-all integrated steam-water void fractions in going from a 4 x 4 array to a 9 x 9 array of rods with the same equivalent diameter.

4.0 GENERAL REVIEW

4.1 Pressure Drops

Single-phase frictional losses for flow in a parallel rod array have been studied experimentally (1) and analytically (2). The results of these efforts indicate that isothermal friction factors (turbulent) for rod bundles will closely follow the Moody (3) round tube relationship using the equivalent diameter concept (only if the pitch to rod diameter ratio is greater than 1.2 for a square pitch array according to (2). Exit, entrance, and joint losses for various types of end fittings and spacing devices were reported by the Bettis Atomic Power Laboratory (1 and 4) for a single-phase flow.

Early studies of two-phase pressure losses were used by Martinelli and Nelson (5) to formulate an empirical correlation for two-phase steam water flows in round tubes at pressures up to the critical value. Recent experiments at the University of Minnesota (6) in horizontal round tubes at pressures from 25 to 1415 psia have indicated a Reynolds number effect different from that in

the Martinelli correlation. A new correlation more accurately describing the Minnesota data has been presented (6).

Data for boiling flows in vertical rectangular ducts at 2000 psi have been reported in (7) and this data also indicates an effect of flow rate over and above that predicted by Martinelli. A family of curves was presented which in a sense could be thought of as adding a mass velocity effect to the Martinelli correlation. This approach was extended (8 and 9) and compared with data for boiling flow in vertical rectangular channels at pressures from 150 to 600 psig with reasonable agreement being observed (particularly at 600 psig).

Two-phase form type losses have been of interest to several investigators as entrance, exit and orifice flow phenomena. An extensive series of air-water experiments has been performed at Argonne National Laboratory, and a survey of available methods for treating two-phase systems was presented by Lottes (10).

One of the earliest reports of boiling pressure drop in a parallel rod array was presented by Bettis Atomic Power Laboratory (11). These data which were for 2000 psia were generally predictable by the family of curves (7), and it was tentatively concluded that the equivalent diameter concept would permit boiling pressure drop in rod arrays and in rectangular ducts to be treated by the same method at least for net steam boiling (bulk boiling).

More recently, additional data have been reported for two-phase (unheated) pressure losses in a parallel rod array including spacer and exit losses at 1000 psia (12). The friction results are represented by simple empirical equations but are reported as being consistent with the Martinelli-Nelson correlation (5) at high mass flow rates. The form type losses are compared with a prediction by Tippets (12) using the void data of Larson (13), and the agreement is not good, particularly at the lower mass flow rates.

The effect of subcooled nucleate boiling (local boiling) has been extensively studied at 2000 psia in rectangular channels and to a lesser extent at lower pressures in the same geometry. Predictive methods were suggested (14). Later studies in round tubes at from 50 to 400 psia were reported (15), and an empirical correlation based upon boiling length was proposed. However, it was conceded that regions close to the entrance must be distinguished from regions in fully established flow.

Local boiling in round tubes from 1100 to 1300 psia has also been extensively studied at Martin (16), and a design equation depending upon the heat transfer coefficient has been recommended.

4.2 Void Fraction

Coincident with the studies of two-phase pressure losses, investigations of void fractions (volumetric fraction of duct occupied by vapor) have been performed. Objectives of these studies have

been to make available the void data for use in interpreting and analyzing two-phase pressure drop data, for calculating the driving head in natural circulating systems, as well as for use in computing moderator densities in nuclear reactors.

In addition to the two-phase pressure losses, Martinelli and Nelson formulated an empirical correlation of void fraction as a function of quality and pressure (5). This correlation indicated that the void fraction was not the same as that computed from the weight fraction and the assumption of a homogeneous mixture of liquid and vapor (homogeneous model, slip ratio of unity). Subsequent experiments and analyses verified the failure of the homogeneous model in many cases, which in turn prompted more experiments and analyses.

A later review of the Martinelli correlation indicated a slight inconsistency with respect to the slip ratio interpretation of void fraction, and the correlation was adjusted to eliminate this difficulty (17).

A survey of the available techniques for measuring void fractions has been published (18), and a detailed discussion of the external source, gamma ray attenuation method was presented (19) and reported in ACNP-63004. The results from an extensive experimental evaluation of this technique were presented (20) for rectangular channel geometry.

Experiments at the University of Minnesota have yielded void for unheated steam water flows in horizontal tubes at 400 to 1000 psi (13). This void data generally falls below the Martinelli curves at steam qualities less than 10 per cent but appear higher than the curves at higher qualities.

The results from an extensive series of experiments performed at Argonne National Laboratory with boiling water in vertical rectangular channels have been summarized (9). These experiments indicate that the void fraction is dependent upon superficial liquid velocity, quality, and pressure with appreciable interaction between effects.

5.0 THEORETICAL CONSIDERATIONS

5.1 Pressure Drops

The phenomenon of a single-phase flow pressure drop in a parallel rod array can be examined by conventional concepts. The frictional losses can be expressed by the form:

$$\Delta P_f = \frac{G^2 f_{iso} L}{2 g_c \rho_f D_e} \qquad (1)$$

where D_e is the conventional equivalent diameter.

Single-phase form losses are often expressed in terms of the velocity head in the constriction.

$$\Delta P = \frac{G_c^2 k_{iso}}{2 g_c \rho_f} \qquad (2)$$

(Where G_c is the mass velocity based upon the area of the constriction.)

If the constriction is accompanied by a net change in area from the upstream region to the downstream region, as for an entrance and/or exit tube sheet, the recoverable part of the form loss may be separated out; for example, an expansion would be given by:

$$\Delta P_{rec} = \frac{G^2}{2g_c \rho_f} (\sigma^2 - 1) \tag{3}$$

where G is based on the area upstream from the constriction and σ is the ratio of upstream to downstream areas.

Thus, $\Delta P = \Delta P_{rec} + \Delta P_{unrec}$

$$\Delta P = \frac{G^2}{2g_c \rho_f} (\sigma^2 - 1) + \frac{k_{iso} G_c^2}{2g_c \rho_f} \tag{4}$$

It is convenient to use the same mass velocity in both the recoverable and unrecoverable terms; defining Σ as the ratio of the constriction area to the upstream area,

$$\Delta P = \frac{G^2}{2g_c \rho_f} \left(\sigma^2 - 1 + \frac{k_{iso}}{\Sigma^2} \right) \tag{5}$$

For boiling flow calculations, the vapor weight fraction (quality) was calculated from the first law of thermodynamics assuming equilibrium.

The approach to two-phase frictional pressure losses has generally been to apply a multiplying factor to the single phase pressure drop. Martinelli (5) proposed that two-phase friction losses could be calculated from single-phase losses by using a multiplier, φ_{LO}^2, in the expression:

$$\Delta P_f = \frac{G^2 f_{iso} L}{2g_c \rho_f D_e} \varphi_{LO}^2 \qquad (6)$$

(The subscript LO on the multiplier refers to the fact that the dynamic head and friction factor are calculated as if all the fluid flowing is flowing as saturated liquid.)

Two-phase form losses are calculated in a variety of ways. Most commonly, use is made of a homogeneous fluid density ($\bar{\rho}_{TP}$), to represent the kinetic energy of the fluid. This technique is really equivalent to using a quality and pressure dependent multiplier since $\bar{\rho}_{TP}$ is only a function of these variables. The first two methods considered in this paper are ramifications of this technique and can be expressed for a form loss with expansion by the following relations:

$$\Delta P = \frac{G^2}{2g_c \bar{\rho}_{TP}} \left(\sigma^2 - 1 + \frac{k_{iso}}{\Sigma^2} \right) \qquad (7)$$

and

$$\Delta P = \frac{G^2}{2g_c \bar{\rho}_{TP}} (\sigma^2 - 1) + \frac{G^2}{2g_c \rho_f} \frac{k_{iso}}{\Sigma^2} \varphi_{LO}^2 \qquad (8)$$

The first relation implies that both the recoverable and unrecoverable two-phase losses stem from phenomena duplicating single-phase effects but with a reduced density. The second equation ascribes a frictional mechanism to the unrecoverable loss, but handles the recoverable part the same as in Equation 7.

Another approach is to consider that for small values of quality all the losses are associated with the liquid phase. To utilize this assumption it is necessary to know the volume fraction occupied by the liquid phase. Using a method similar to that of Lottes (10), the following expression (again for a net expansion) can be written:

$$\Delta P = \frac{G^2}{2g_c\, \rho_f\, (1 - Rg)^2} \left(\frac{k_{iso}}{\Sigma^2} + \sigma^2 - 1 \right) \qquad (9)$$

5.2 Void Fraction

The theoretical basis for the gamma attenuation void measuring technique has been treated in considerable detail by Petrick (21) and by Hooker and Popper (19), and only a brief review will be presented. The principal assumptions used are as follows:

1. The gamma beam consists of parallel rays and is very thin.
2. The beam is monoenergetic (the source in this case is Cesium 137).
3. The attenuation is exponential with distance and material density.

The attenuation of the gamma beam is given by:

$$N/N^* = e^{-\beta X} \tag{10}$$

where N/N^* is the fraction of incident radiation penetrating a distance X in the attenuating material. The linear attenuation coefficient, β, is assumed to be dependent only upon the nature of the material, density, and radiation energy.

If the radiation intensity (per unit area) is measured from a duct containing a given permanent structure and completely filled with vapor, Equation 10 becomes:

$$N_v/N^* = e^{-\beta_v X_e - \beta_s X_s} \tag{11}$$

A similar measurement obtained at the same position with the duct filled with liquid would be represented by:

$$N_L/N^* = e^{-\beta_L X_e - \beta_s X_s} \tag{12}$$

Finally, a measurement obtained with the duct filled partly with liquid and partly with vapor would be represented by:

$$N_{TP}/N^* = e^{-\beta_L X_{Le} - \beta_v X_{ve} - \beta_s X_s} \tag{13}$$

Thus, the fraction of fluid present in the thin beam as liquid becomes:

$$\frac{X_L}{X} = \frac{\ln N_v/N^* - \ln N_{TP}/N^*}{\ln N_v/N^* - \ln N_L/N^*} = \frac{\ln N_v/N_{TP}}{\ln N_v/N_L} \tag{14}$$

and the fraction of fluid present as vapor becomes:

$$\frac{X_v}{X} = \frac{\ln N_{TP}/N_L}{\ln N_v/N_L} \tag{14a}$$

if the attenuation coefficients are assumed to be the same in the completely filled and partially filled conditions (and the decay of the source is neglected). Note that with this assumption (and those preceding), it is possible to measure a local liquid fraction (and/or void fraction since $X_v/X = 1 - X_L/X$) by performing three radiation measurements at the location of interest without ever being committed to a certain value or set of values for the attenuation coefficients.

Although the development of the theory has utilized a radiation intensity measurement with the duct full of vapor, it is often permissible to substitute a measurement with the duct full of air. This is the case in the present experiments wherein the typical attenuation coefficients for the saturated water were found to be about 0.166 in^{-1}. Assuming that the coefficient for the same material is proportional to the density, corresponding coefficients for saturated steam at 600 psi would be about 0.00432 in^{-1} or a factor of 38.3 lower. Thus, substituting an air measurement for a vapor measurement causes the experimental void determinations to be low by about 2.6 per cent (relative). This is considered to be well within the experimental accuracy of the measuring system.

With respect to the ultimate application of the void data, it is desirable to determine the mean void fraction in the duct cross section. This can be accomplished by performing a series of local measurements at different positions and then integrating the results.

i.e.

$$\bar{R}_g = \frac{\int R_g X dy}{\int X dy} \qquad (15)$$

Perhaps the most important assumption in the foregoing discussion is that of a very narrow beam. This assumption was investigated in (22) using a digital computer program. Variations in the thicknesses of attenuating materials across the beam width were found to produce significant errors for an aluminum-Lucite model with a Thulium source. However, the use of Cesium was found to virtually eliminate such errors in a steel, water system due to the reduced attenuation in the water. Based upon the results in (22), the over-all error of the present void measuring system is about $\pm$ 10 per cent relative void fraction for voids of about 50 per cent.

During the present experiments, a discriminator was utilized to eliminate the "noise". Simple experiments using Lucite blocks were used to establish the discriminator settings which maximized the signal-to-noise ratio, and the exponential nature of the attenuation was closely verified.

6.0 AXIAL PRESSURE PROFILE DOWNSTREAM FROM A SPACER, SINGLE-PHASE FLOW EXPERIMENT

6.1 Equipment

A prototype of the Pathfinder boiler fuel element was used to examine the axial pressure profile occurring in parallel rod flow with spacers.

The element was 6 ft long and consisted of a 9 x 9 array of rods on a 0.535 inch square pitch. The rods comprising the upper half (3 ft) of the element were 0.367 in. diameter (pitch to diameter ratio of 1.46) and the rods in the lower half were 0.409 in. diameter (pitch to diameter ratio of 1.31). The reduction in rod size in the top half compensates for moderator voiding during power operation. The rods were fixed at both ends in small grid plates, and intermittent "tube sheet" type spacers were used at 18 in. intervals. In order to facilitate flow visualization studies, the element containment box was fabricated from Lucite.

The element was installed in a low pressure flow loop and heavily instrumented with pressure taps connected to a bank of manometers. A schematic of the low pressure loop is shown in Fig. 1. Pressure taps were located every two inches downstream from the first three spacers to give an accurate description of the axial pressure profile. Fig. 2 shows the test installation.

The experiments were run at approximately atmospheric pressure using room temperature water. Flow rates were varied from 134,000

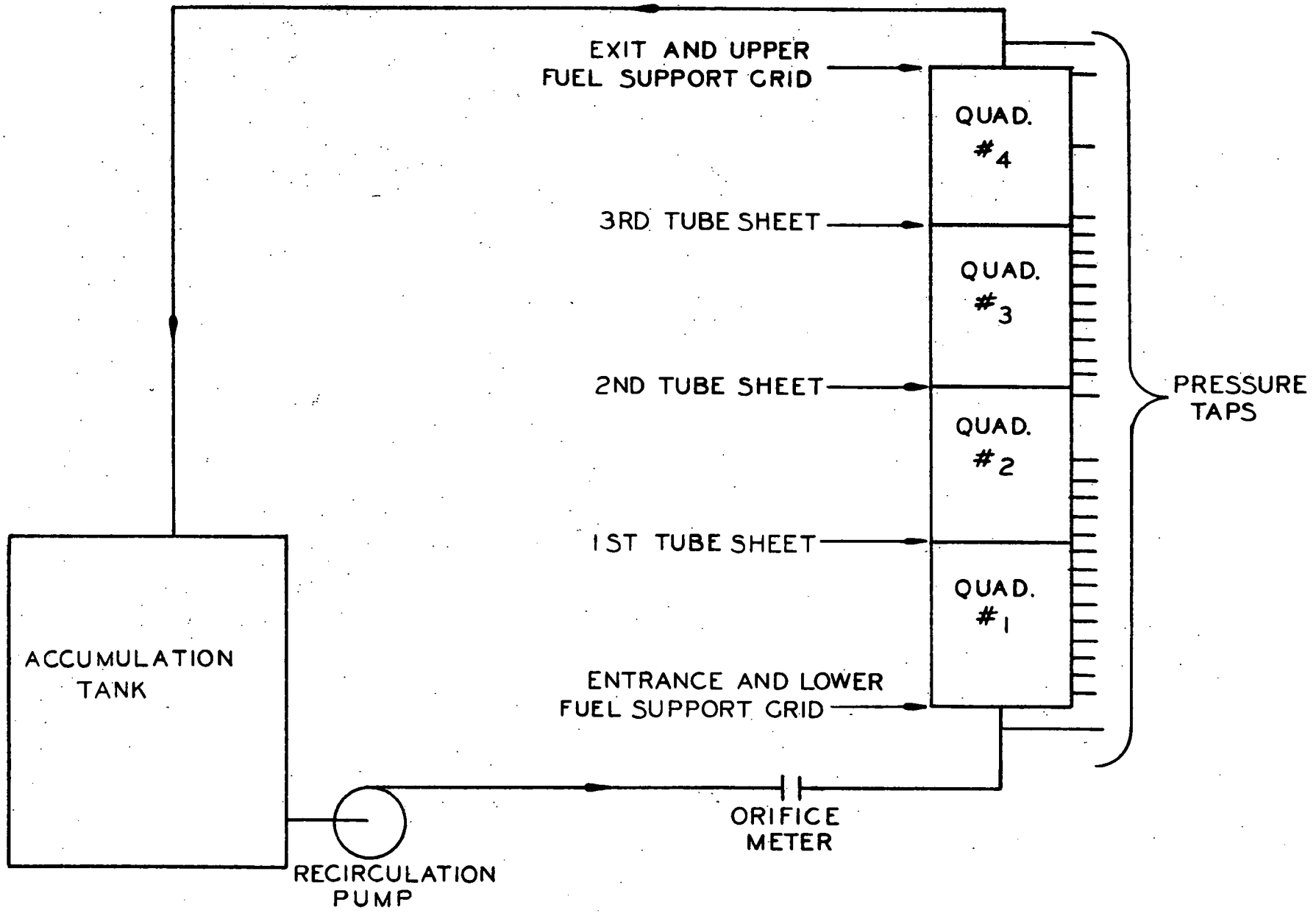

Figure 1 - Low Pressure Loop Schematic Diagram (43-024-826)

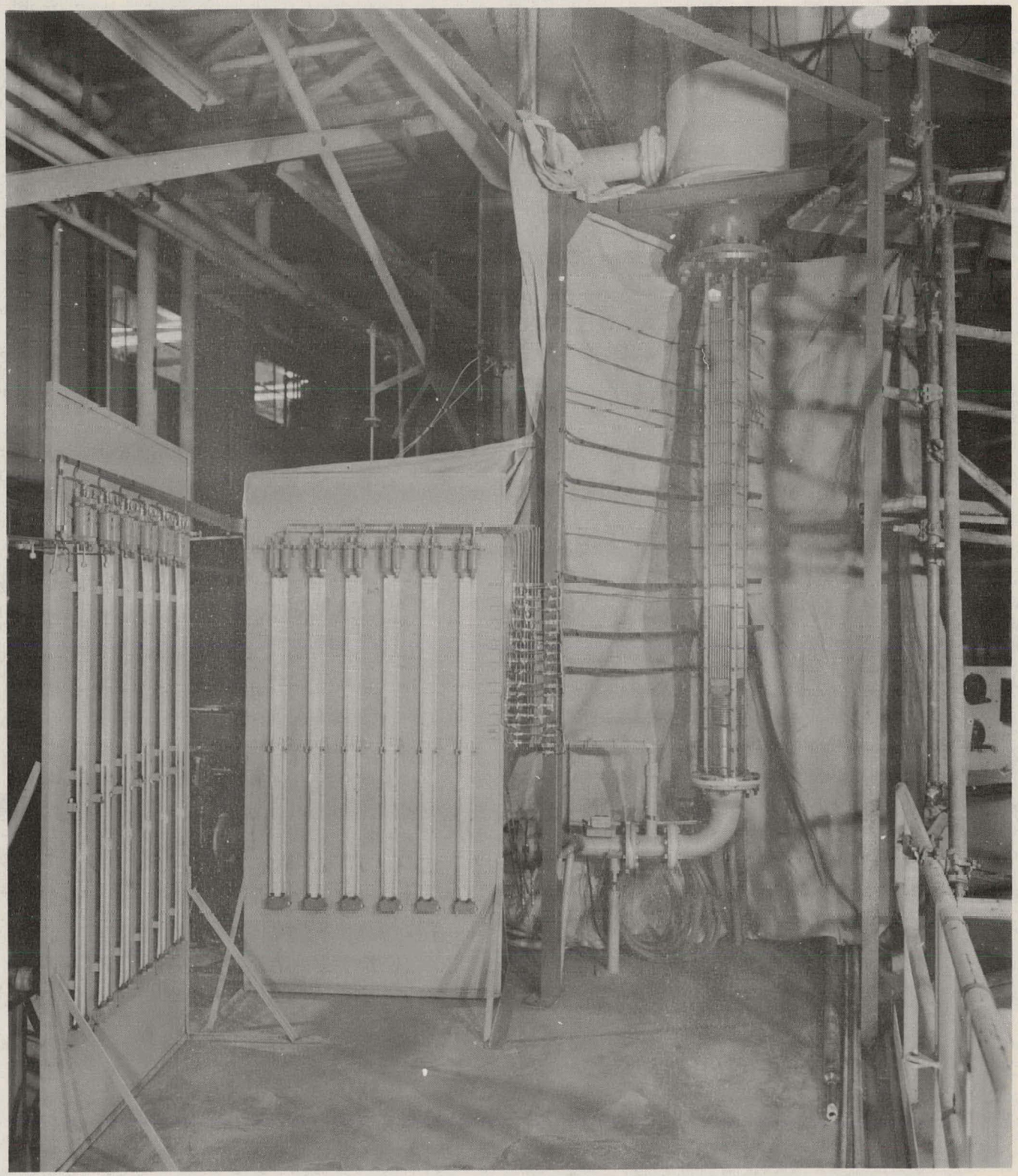

Figure 2 - Low Pressure Air-Water Loop (21583)

to 342,000 lb/hr, which corresponds to mass velocities (G) of 1.3×10^6 to 3.4×10^6 lb/hr-ft^2. Flow rates were determined by using a calibrated orifice meter in the recirculation piping.

Because the fuel element containment box was made of Lucite, there was some concern as to the amount of lateral expansion which would occur at the higher flow rates and create a positive pressure inside the box. However, by using steel supports in the Lucite wall every six inches along the axial length of the test section, the measured expansion was held to less than 0.010 in.

6.2 Axial Pressure Profiles

Sample plots of pressure drop vs. length are shown in Fig. 3. It can be seen that $\Delta P/\Delta L$ is not linear, as it should be for established friction, in the first few inches of quadrant I. In this quadrant, there is little or no drop in static pressure for about 10 equivalent diameters. Then the pressure is seen to fall linearly but at a rate much less than expected for friction. This phenomenon is attributed to the hydraulic effects of the fuel support grid (inlet grid) being dissipated over the complete length of the quadrant. It is seen that the pressure loss in this grid is nearly an order of magnitude larger than the other tube sheet losses; following these downstream constrictions, conventional friction losses are quickly established.

The data for the first quadrant show that application of the common method of determining form losses for end fittings by subtracting

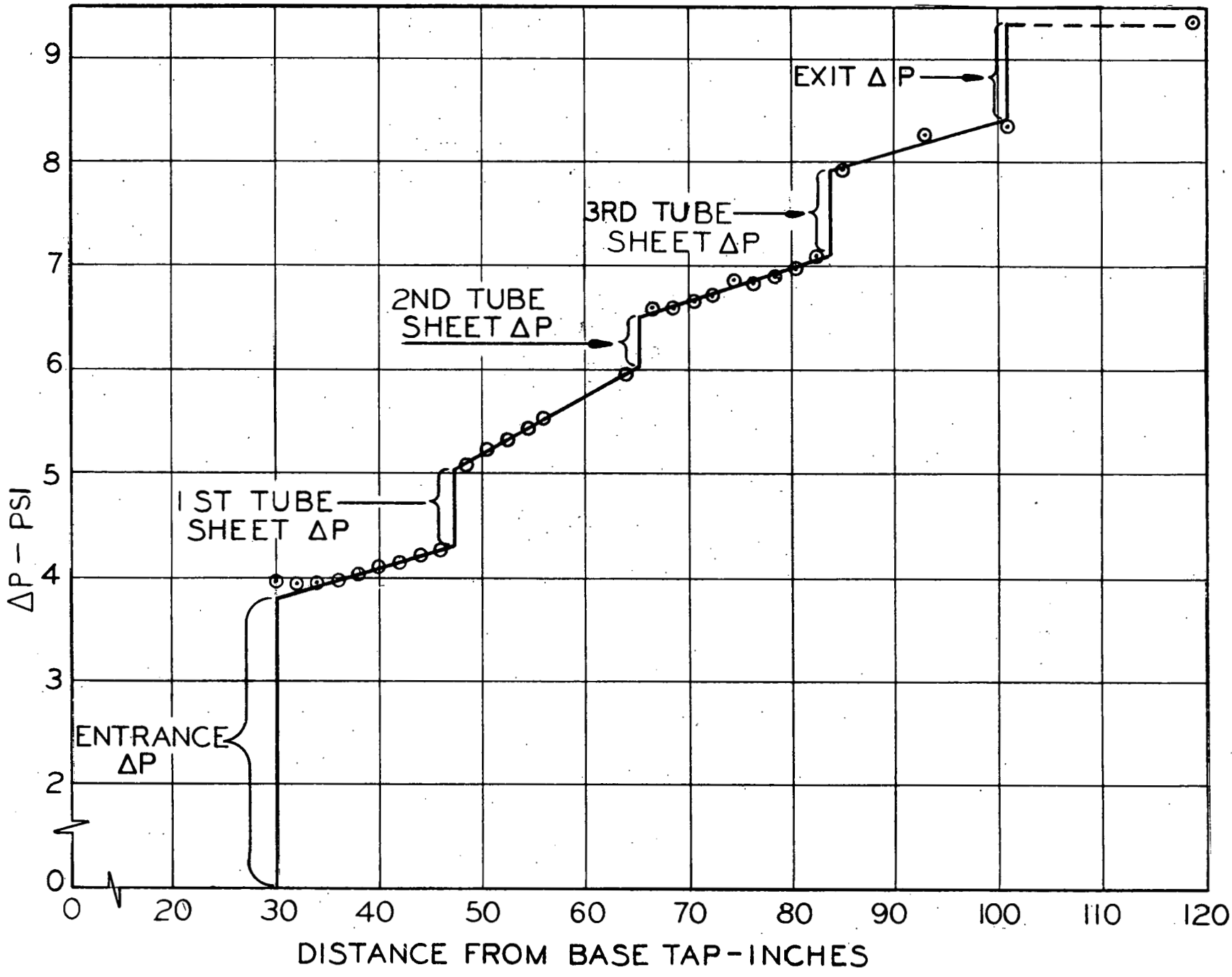

Figure 3 - Boiler Prototype Element Sample Over-all Pressure Drop (43-024-829)

calculated friction from measurements of over-all pressure drop would yield unrealistic results.

6.3 Friction Factors

Friction factors over the 81 rod array were calculated for the quadrants which had taps that were spaced every 2 in. This was accomplished by plotting the frictional pressure drop versus length and finding the slope $\Delta P_f/\Delta L$. Then the friction factor (f) was calculated from the equation:

$$f = \frac{\Delta P_f}{\Delta L} \frac{De\ 2g_c\ P}{G^2}$$

The data from quadrant 4 were not reduced to friction factors because that quadrant was not heavily instrumented.

In calculating f, $\Delta P_f/\Delta L$ was taken as the slope which best fit the downstream points in the quadrant. Equivalent friction factors were similarly calculated for the linear portion of the first quadrant. The friction factors are shown graphically in Fig. 4 in comparison with the smooth Moody curve (3). The agreement is good except for the data from quadrant 1 which range from 15 to 50 per cent below the Moody curve due to the distorted profile which occurred downstream from the first supporting grid.

6.4 Form Loss Coefficients

The entrance, exit, and tube sheet pressure drops were converted to unrecoverable form loss coefficients by the Equation 4. Mass

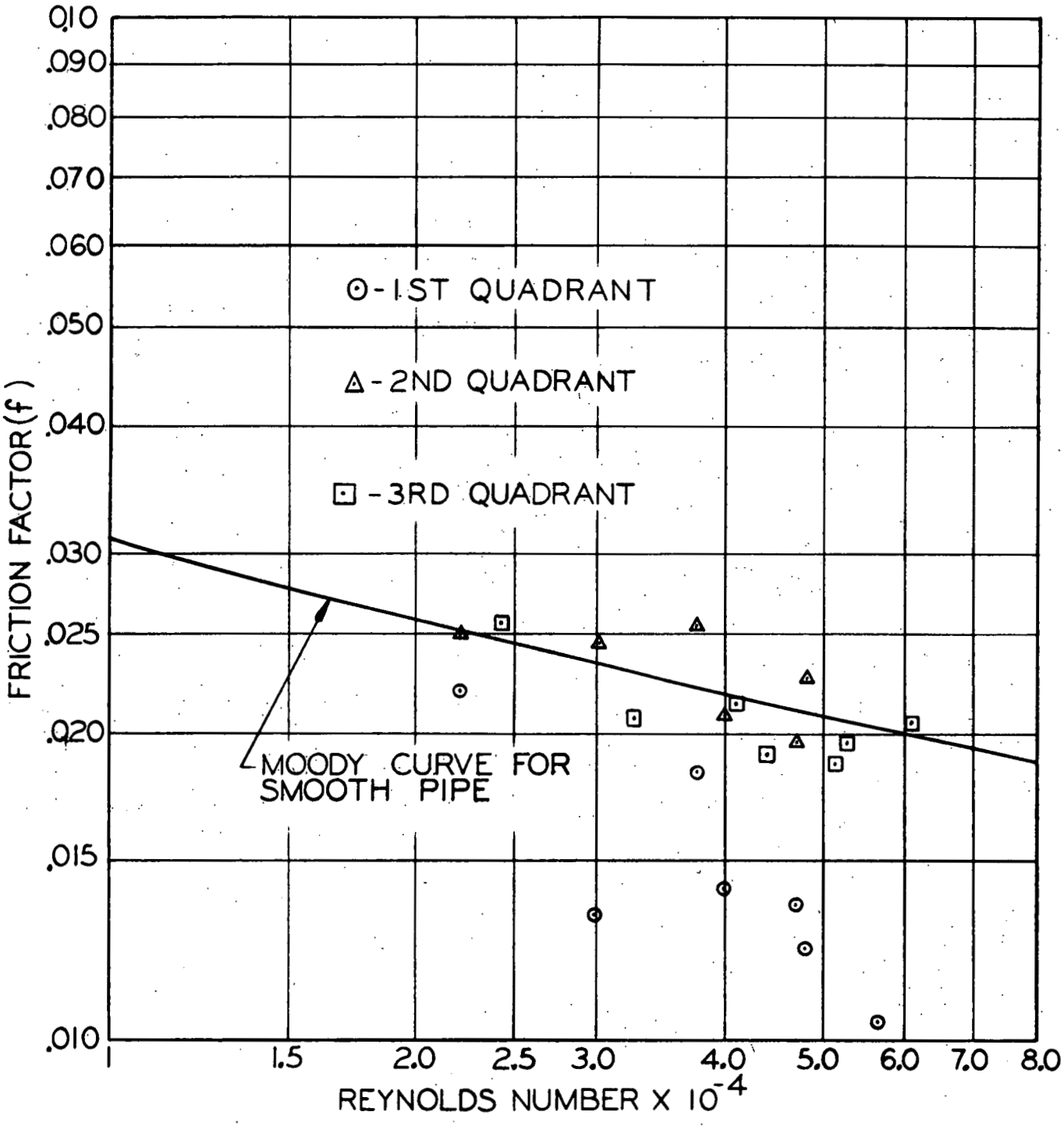

Figure 4 - Boiler Prototype Element Isothermal Friction Factors (43-024-828)

velocity (G_c) was based on the area of the constriction for the tube sheets, and the flow area among the tubes for the inlet and exit losses. The form loss P was arrived at by extending the friction pressure drop line back to the tube sheet (Fig. 3). By using this procedure, the distorted profile immediately behind the grids and tube sheets was neglected. It is noted that these backward extrapolations were based upon the experimental pressure profile data and not on a calculated frictional gradient. The entrance, exit, and tube sheet unrecoverable loss coefficients for the final design configurations are plotted versus Reynolds number in Figures 5 and 6. The entrance and exit loss coefficients (Fig. 5) cannot be readily compared with the Bettis data (4) since their entrance and exit losses were combined into over-all values. However, the tube sheet coefficients (Fig. 6) are in reasonable agreement with the joint loss coefficients reported for the "egg crate" type connection which is similar to that employed in the present study.

6.5 Conclusions

1. The axial pressure profile was found to be very nearly linear immediately downstream (1 or 2 equivalent diameters) from all the spacers except at the inlet.
2. Examination of the region downstream from the inlet grid showed that the flow is not fully established over the entire quadrant length (40 equivalent diameters).

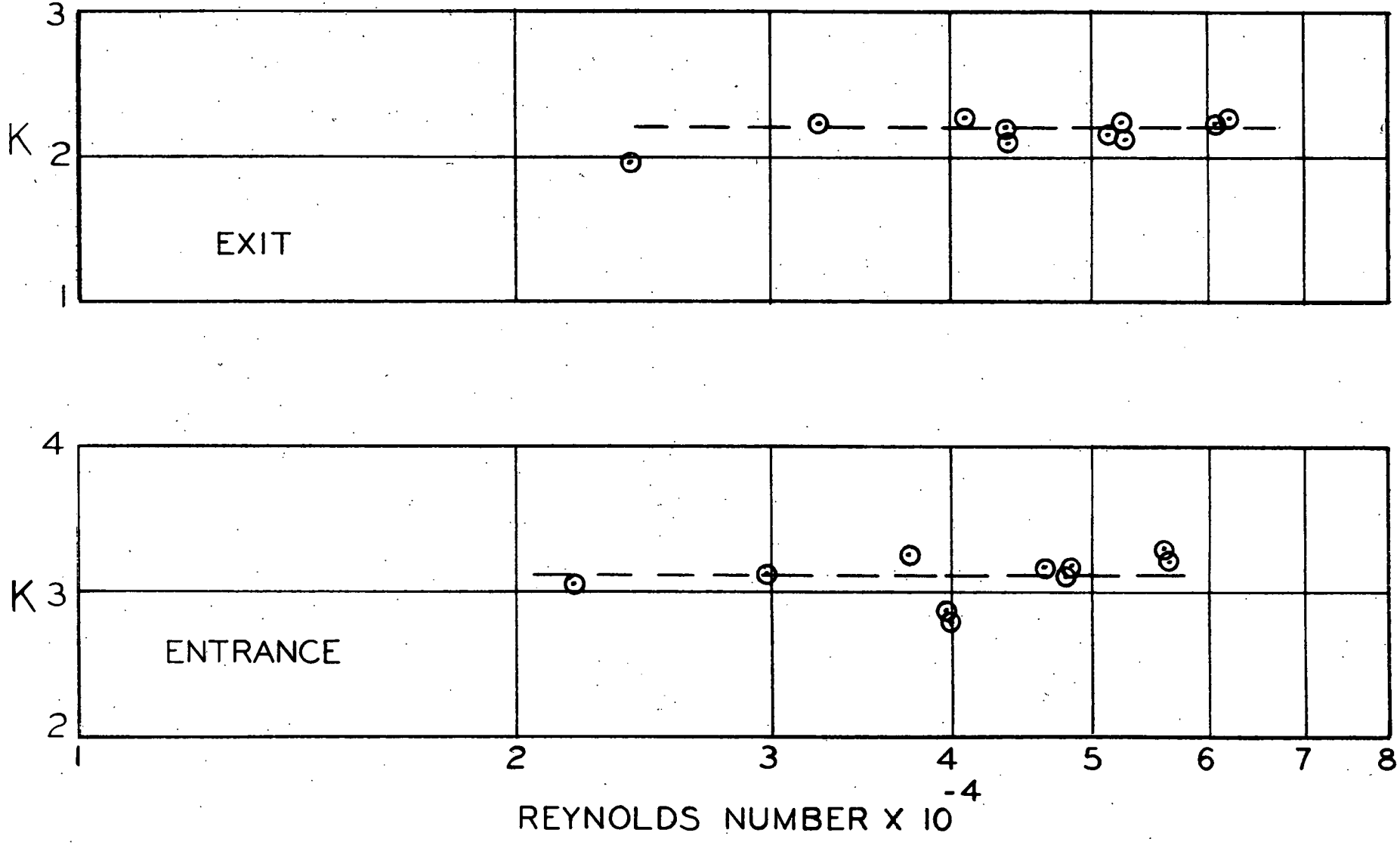

Figure 5 - Entrance and Exit Form Loss Coefficients (43-024-830)

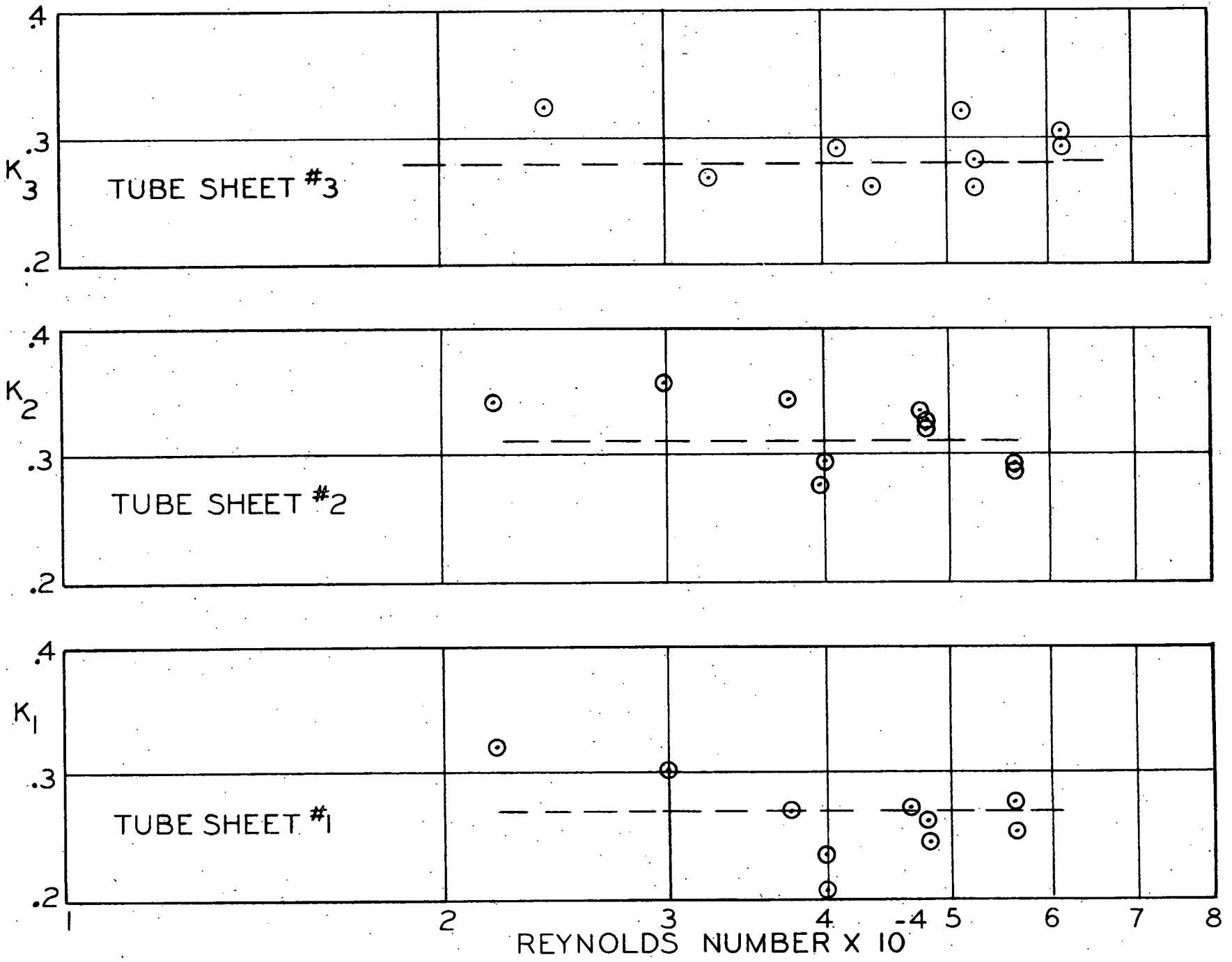

Figure 6 - Tube Sheet Form Loss Coefficients (43-024-831)

3. The fully established friction factors are in good agreement with the Moody curve (3), and the tube sheet loss coefficients are in reasonable agreement with similar data presented in (4).

7.0 PRESSURE PROFILE DOWNSTREAM OF A SPACER IN TWO-PHASE FLOW EXPERIMENT

7.1 Equipment

The equipment used to perform this study included the same low pressure loop with the prototype Pathfinder boiler element described earlier with the addition of an air supply. An air line from a rotary type compressor supplied air to the loop piping 3 feet ahead of the test sections lower flange (Fig. 2). Air flow rates were determined by using a Laminar flow metering device.

7.2 Test Conditions

Mass flow rates were varied from 1.37×10^6 to 2.32×10^6 lb/hr-ft^2 with an air-water mixture at room temperature. The mass fraction of air flowing (quality) was varied from 0.142 per cent to 0.263 per cent (corresponding to void fractions from 0.37 to 0.69 by the homogeneous model).

7.3 Pressure Profiles

Figures 7 and 8 show two sample axial pressure profiles for air-water mixtures flowing in the element. As in the case of all water flow, the profile downstream of the lower grid shows some effects of the grid for 10 - 12 equivalent diameters downstream. However,

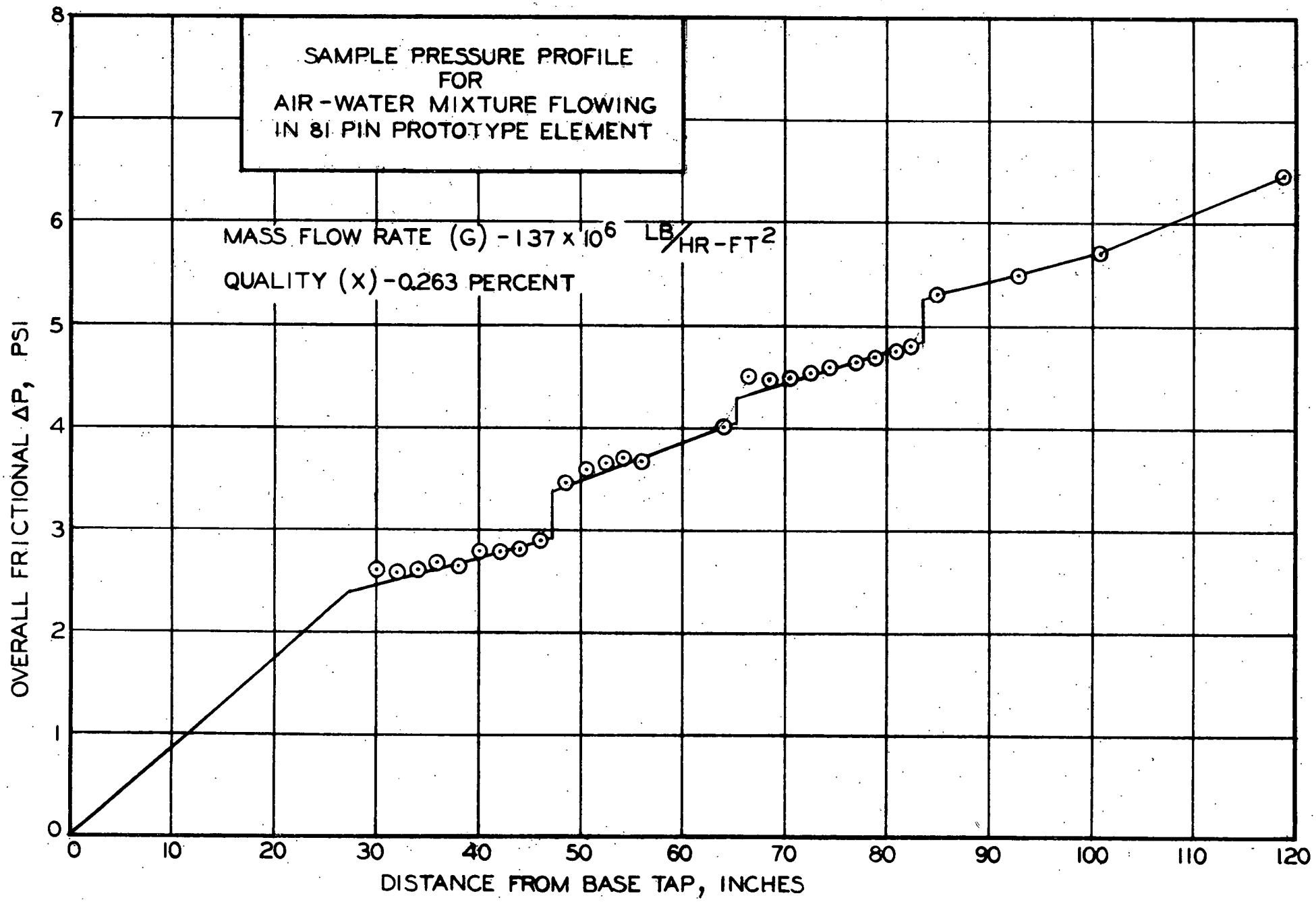

Figure 7 - Sample Pressure Profile for Air-Water Mixture Flowing in an 81 Pin Prototype Element (43-024-983)

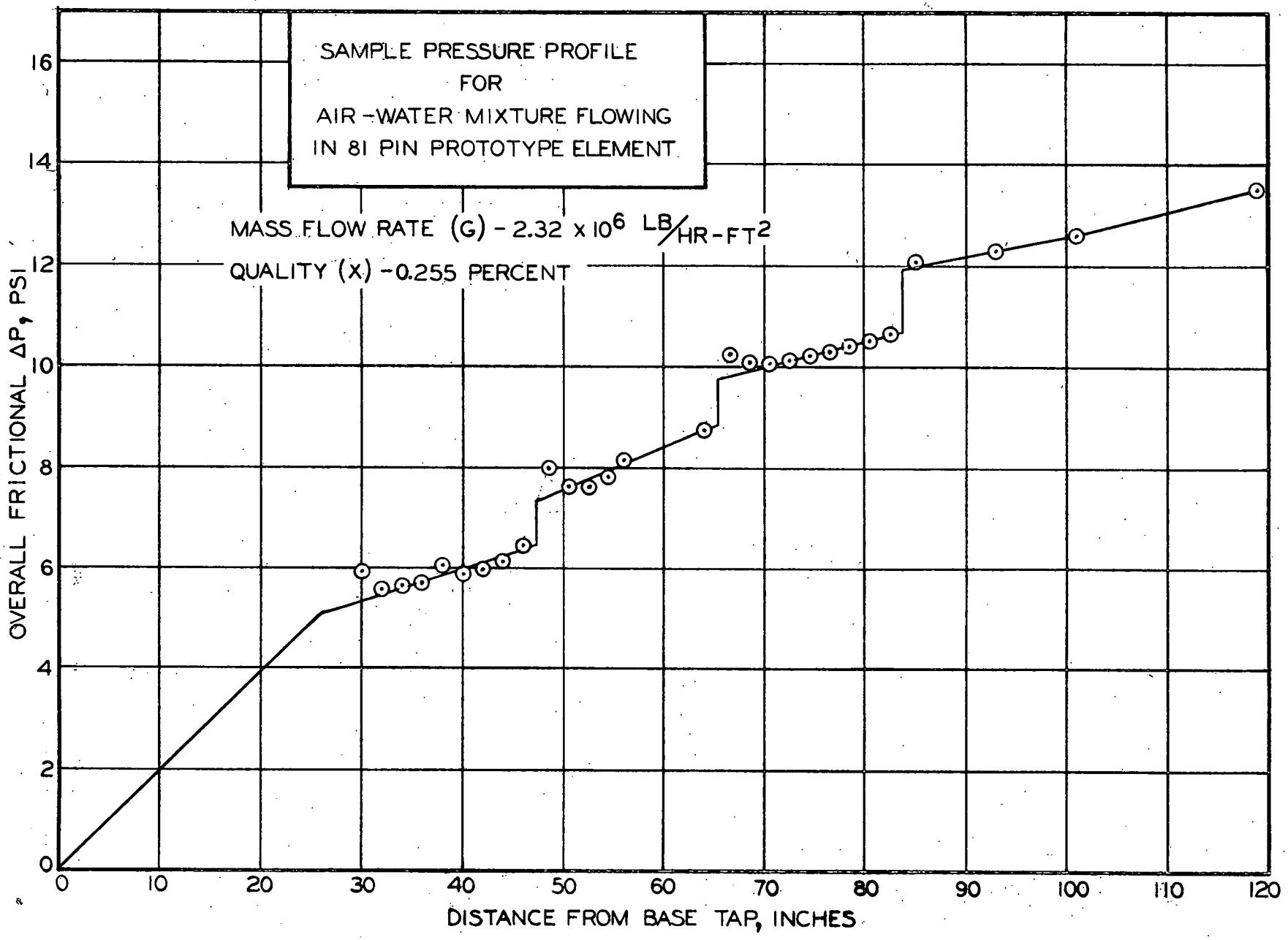

Figure 8 - Sample Pressure Profile for Air-Water Mixture Flowing in an 81 Pin Prototype Element (43-024-924)

the air-water data also shows this type of effect behind tube sheets 1 and 2. This effect may be due to two-phase effects or merely the result of having a larger pressure loss through the tube sheets. In other words, the two-phase flow field may take longer to become fully established than for single-phase flow although the difference is not great. Also the higher pressure losses encountered with the two-phase case implies the existence of a greater disturbance and this may partially explain the downstream effects.

7.4 Loss Coefficients

As expected, the loss coefficients for the two-phase case were greater than in the single-phase case. The ratio of two-phase to single-phase loss coefficients measured in these experiments was correlated by using the ratio of single-phase to average two-phase density ($\rho_f/\bar{\rho}_{TP}$), and the results are shown graphically in Figures 9 and 10. The 45 degree lines on these graphs represent Equation 7 so the agreement of the data with the lines is an evaluation of the applicability of Equation 7.

7.5 Friction Factors

After reducing the pressure drops to friction only, by subtracting out the elevation and acceleration portions (using the homogeneous model), friction factors were calculated for the lengths between spacers as in the single-phase tests by taking the slope of the pressure drop versus length curve. These friction factors were

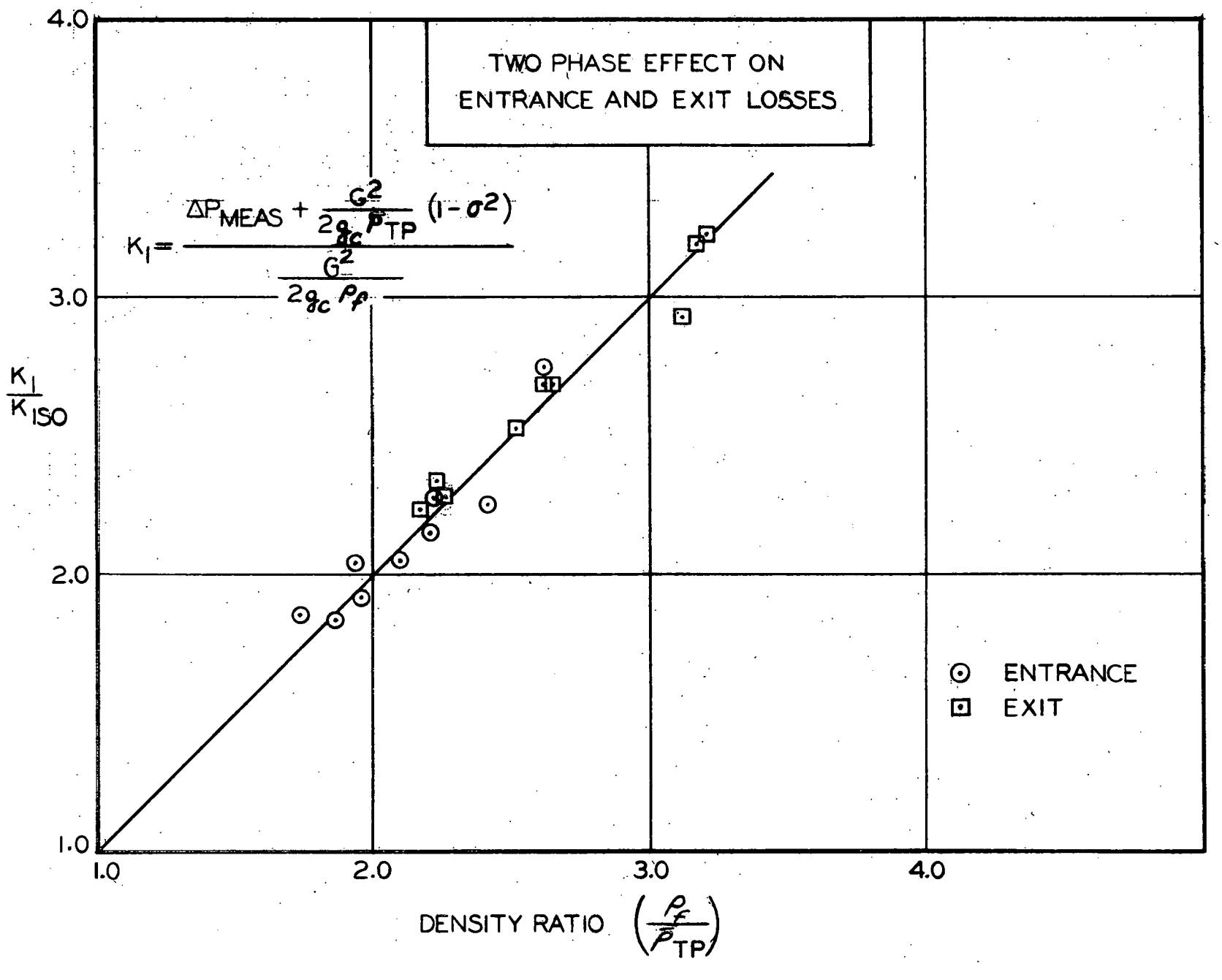

Figure 9 - Two-Phase Effect on Entrance and Exit Losses (43-024-982)

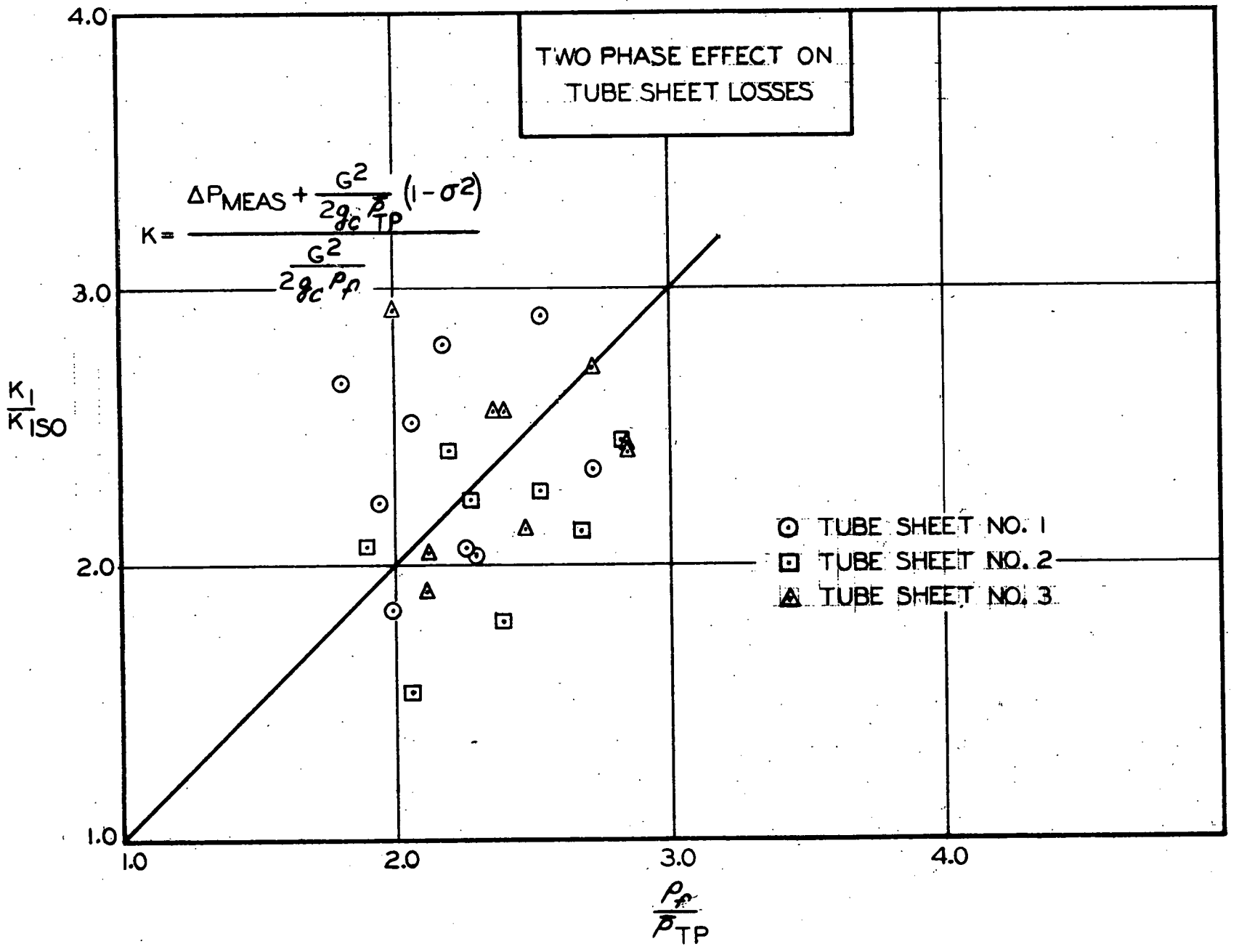

Figure 10 - Two-Phase Effect on Tube Sheet Losses (43-024-980)

then converted to two-phase multipliers by ratioing them to the experimental single-phase friction factors. These multipliers are shown in Figure 11 in comparison with the Lockhart-Martinelli correlation (23). The multipliers being reported are generally considerably lower than the Martinelli values. While no quantitative effect of flow can be deduced from Figure 11, there does seem to be a trend for increasing flow to correspond to a reduction in ϕ_{LO}^2 for the same quality. Without further exploring the possibility of this flow dependency, it is difficult to assess the apparent "scatter" exhibited on Figure 11.

7.6 Conclusions

1. The axial pressure profile downstream from the spacers was found to be similar to the single-phase results, but the pressure gradients did not seem to become well established quite as rapidly.
2. The two-phase multipliers in the first quadrant, wherein the flow was found to be unestablished over the full length, are in agreement with the multipliers for the downstream quadrants, wherein the flow quickly became established.
3. The two-phase multipliers are not in good agreement with the Lockhart-Martinelli correlation (23), but the two-phase form losses are fairly well described by Equation 7.

8.0 BOILING PRESSURE DROPS AND VOID FRACTIONS IN A 4 X 4 ARRAY EXPERIMENT

8.1 Equipment

8.1.1 Heat Transfer Loop

The Heat Transfer Loop located at the Greendale Lab was designed for investigation of heat transfer and pressure drop problems in nuclear reactors. The loop is also instrumented to enable investigation of burnout and void fraction. Multiple valve arrangements provide for forced or natural circulation flow. The use of a steam separator above the boiling test section provides saturated steam for superheat studies. Nuclear heating is simulated by electrical resistance heating with d-c power available up to 2.25 mw. The loop is rated at 1500 psi, 1000 F. The recirculation flow capacity of the loop is 600 gpm. A schematic diagram of the loop is shown in Figure 12.

8.1.2 Test Section

The 16 pin test section was designed to simulate a Pathfinder boiler fuel element. The test section was 6 ft long and consisted of a 4 x 4 array of stainless steel heater tubes arranged on a 0.570 in. pitch. The tube dimensions were 0.416 in. o.d. (pitch to diameter ratio of 1.37) with a 0.027 in. wall in the lower half of the bundle and 0.367 in. o.d. (pitch to diameter ratio of 1.55) with a 0.065 in. wall in the upper half. This feature corresponds to the Pathfinder design wherein additional flow area is provided in the upper

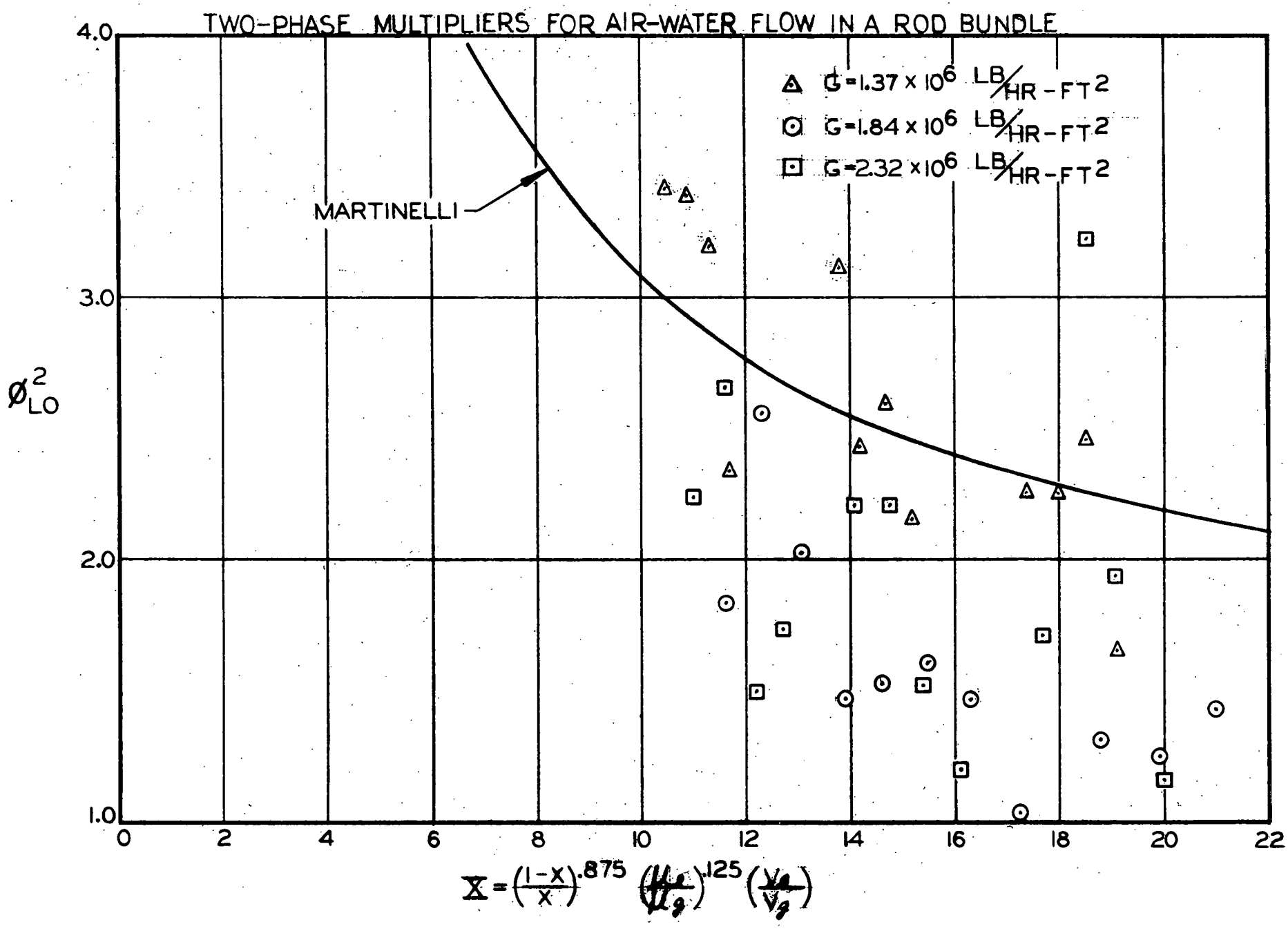

Figure 11 - Two Phase Multipliers for Air-Water Flow in a Rod Bundle (43-024-981)

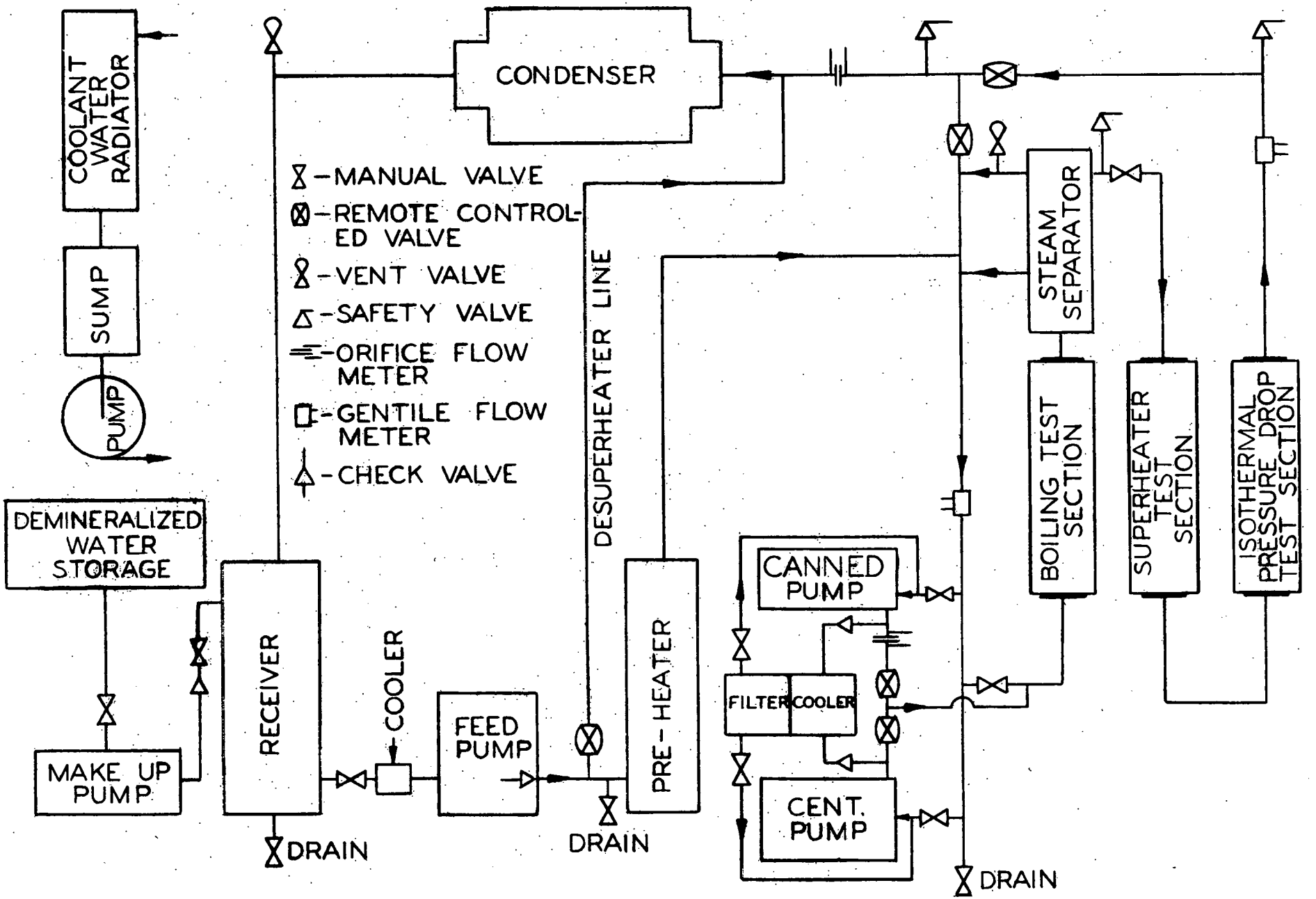

Figure 12 - Heat Transfer Loop Schematic Diagram (43-024-777)

half of the core to offset void effects. The power produced in the upper half is approximately 35 per cent of the total. The tube array was enclosed in a square pressure housing consisting of a 16 gauge stainless steel liner inside a 5/8 in. thick carbon steel box. The flow channel dimension was 2.399 in. square. Figure 13 is a schematic assembly of the test section. Figure 14 is a cross section view of the bundle array showing the spacer and pressure tap assembly.

Spacing of the heated rods was accomplished by using short pieces of 0.148 in. o.d. stainless steel tube with smaller diameter rod inserted down the center to the tube and through holes drilled in the heated rods. Figure 15 shows the assembly. The end connections were simply square grids made of copper bars which were soldered to the stainless rods, and served to center the bundle in the box at each end. These copper bars were 1/8 in. thick x 1/2 in. deep and extended the length of a row or rods. The bundle was also centered in the box at the axial mid-point by four small, electrically isolated, steel rods penetrating the box enclosure and guiding the pin rows adjacent to the bundle center.

Fourteen pressure taps were used to measure the frictional and spacer pressure drops along the length of the test sections. Figure 13 shows the axial spacing of the pressure taps in relation to the rod bundle.

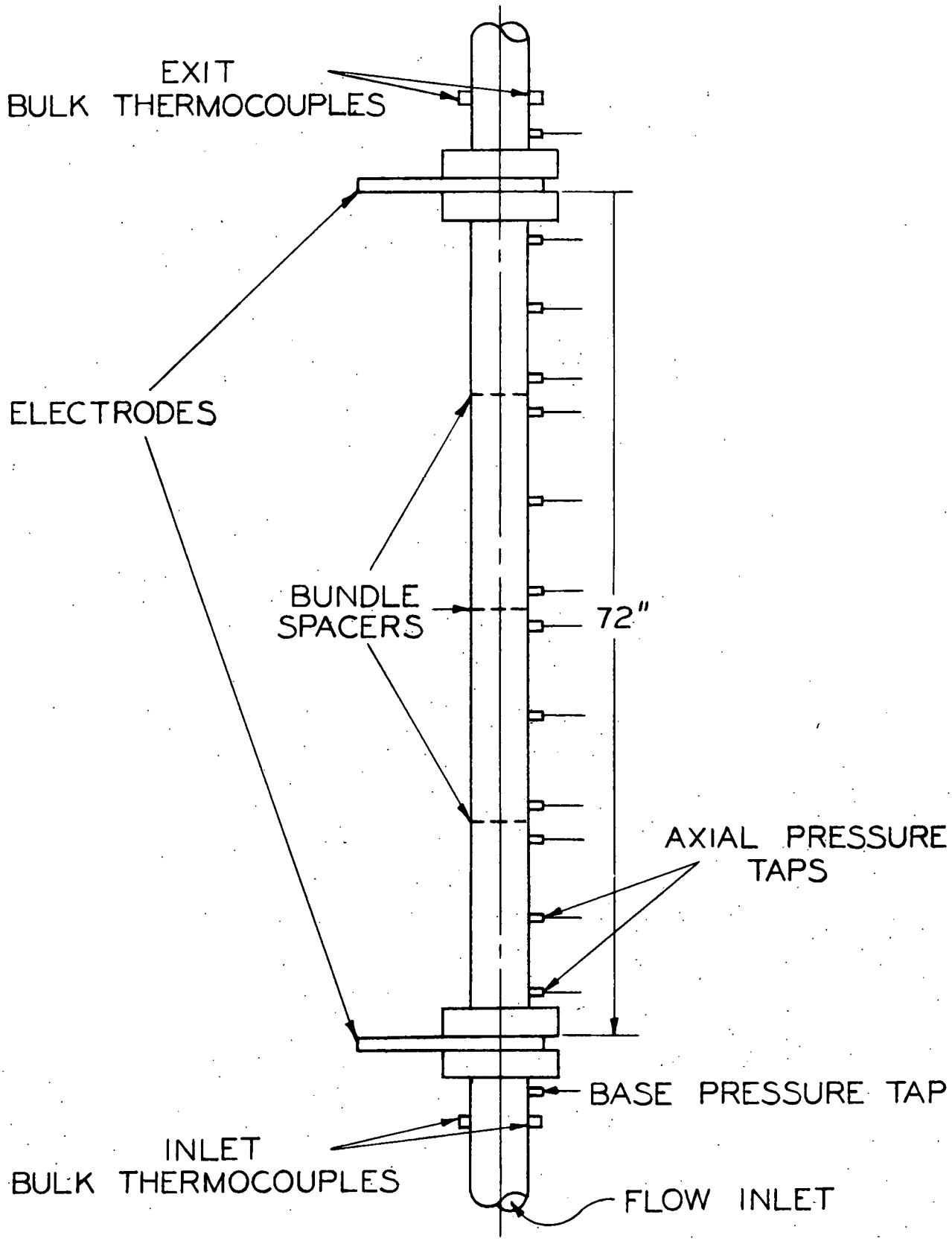

Figure 13 - Sixteen Pin Test Section Assembly (43-024-776)

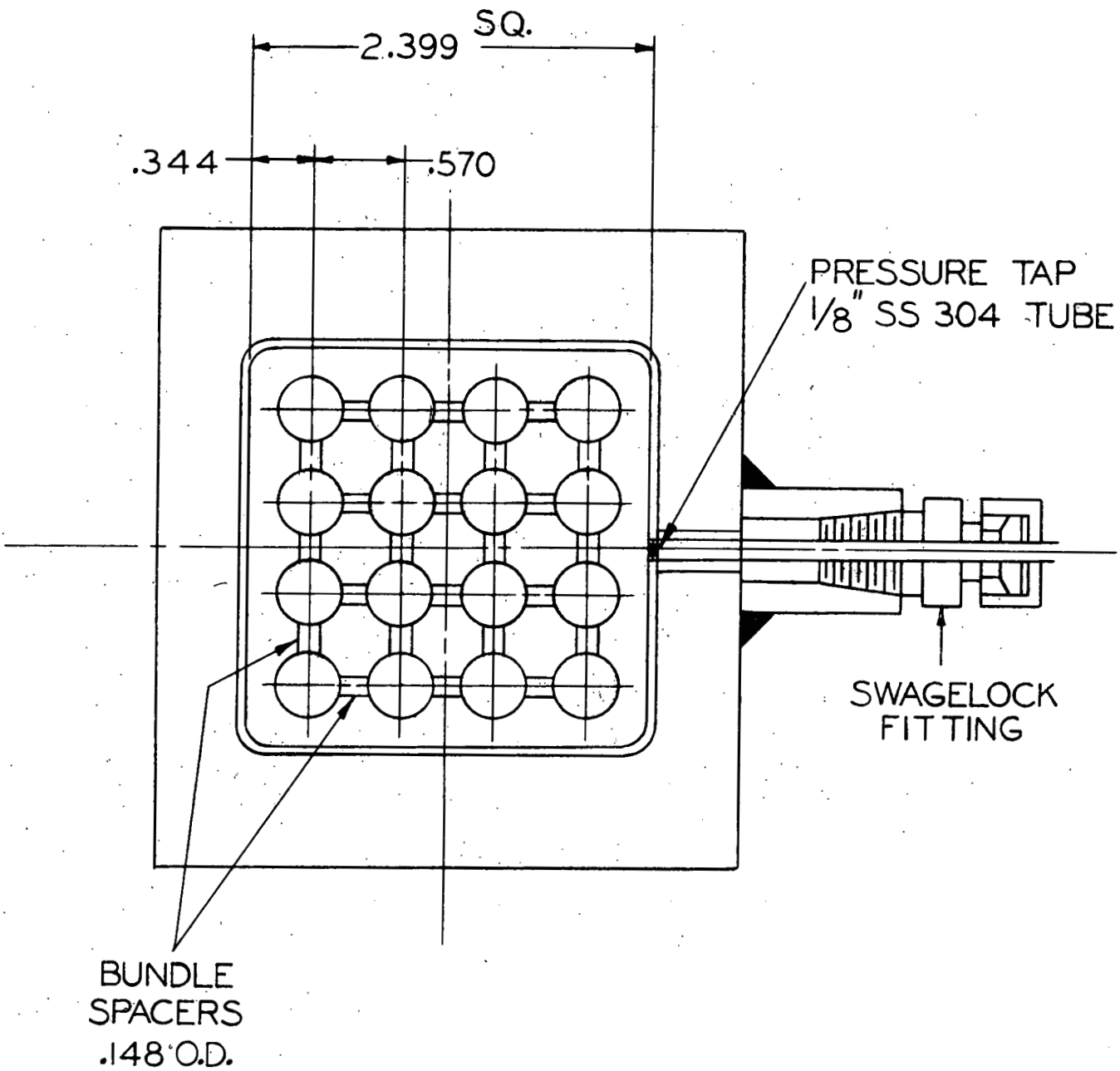

Figure 14 - Cross Section of 16 Pin Test Section (43-024-778)

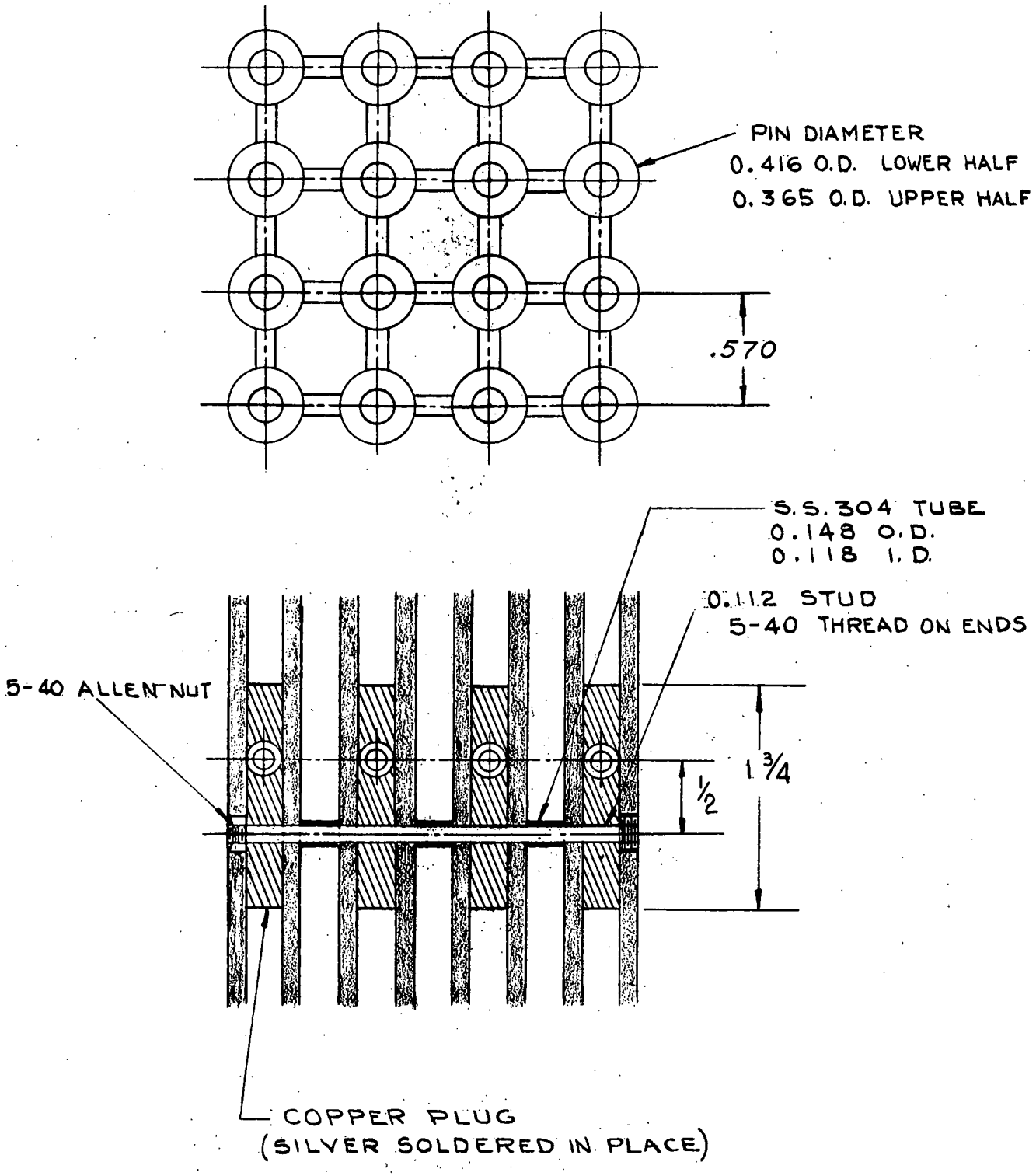

Figure 15 - Pin Bundle Spacer Arrangement (43-024-986)

Bulk coolant temperatures were measured with bare-wire chromel-alumel thermocouples located before and after the test section.

Slots, 1" x 2" x 5/16" deep, were milled in the sides of the box at three axial locations. This was done in order to reduce the required intensity of the source used for the void measurements.

8.1.3 Loop Instrumentation

8.1.3.1 Flow Measurement

Flow rate through the test section was determined by measuring the pressure drop through a 4 in. Gentile flow tube. A 50 in. - 2000 psi well-type manometer was used to measure the pressure drop. The indicating fluid was mercury.

8.1.3.2 System Pressure

The system pressure was measured with a Heise, Bourdon tube type gage. The gage had 1 psi increments from 0 - 1500 psi, and was calibrated with a dead-weight tester before and after the test.

8.1.3.3 Differential Pressure Drops

Differential pressure drops were measured with a bank of 12, 60 in., 2000 psi manometers. The indicating fluid was Meriam #3 with a specific gravity of 2.95.

8.1.3.4 Bulk Temperature Measurements

Temperatures were measured with a Wheelco, 16 point, recording potentiometer calibrated in millivolts. The recorder had a 10 in. chart with a range of 0 - 50 mv d-c in 2.5 mv steps. An ice-water mixture was used for the reference junctions.

8.1.3.5 Test Section Power

The voltage drop across the test section was measured with a Wheelco recording voltmeter. The instrument had a range of 0 - 75 mv d-c in 25 volt steps. A Wheelco recording potentiometer with a range of 0 - 75 mv d-c in 0 - 25 mv steps, and a calibrated 50 mv shunt were used to determine the current.

8.1.4 Void Fraction Equipment

The encapsulated Cesium 137 source of 2.5 curies was housed in a lead pig with a 0.25 in. i.d. aperture, 4 in. long facing the test section. The pig was 8 in. o.d., 8 in. long and weighed about 180 lb and provided acceptable radiation levels at contact with the surface. The Cesium has a half-life of 30 yr which eliminated concern over source decay.

A block diagram of the void measuring system layout is shown in Figure 16. Collimation of the gamma beam was effected by using a 2.5 in. long lead cylinder with a 0.035" x 0.625"

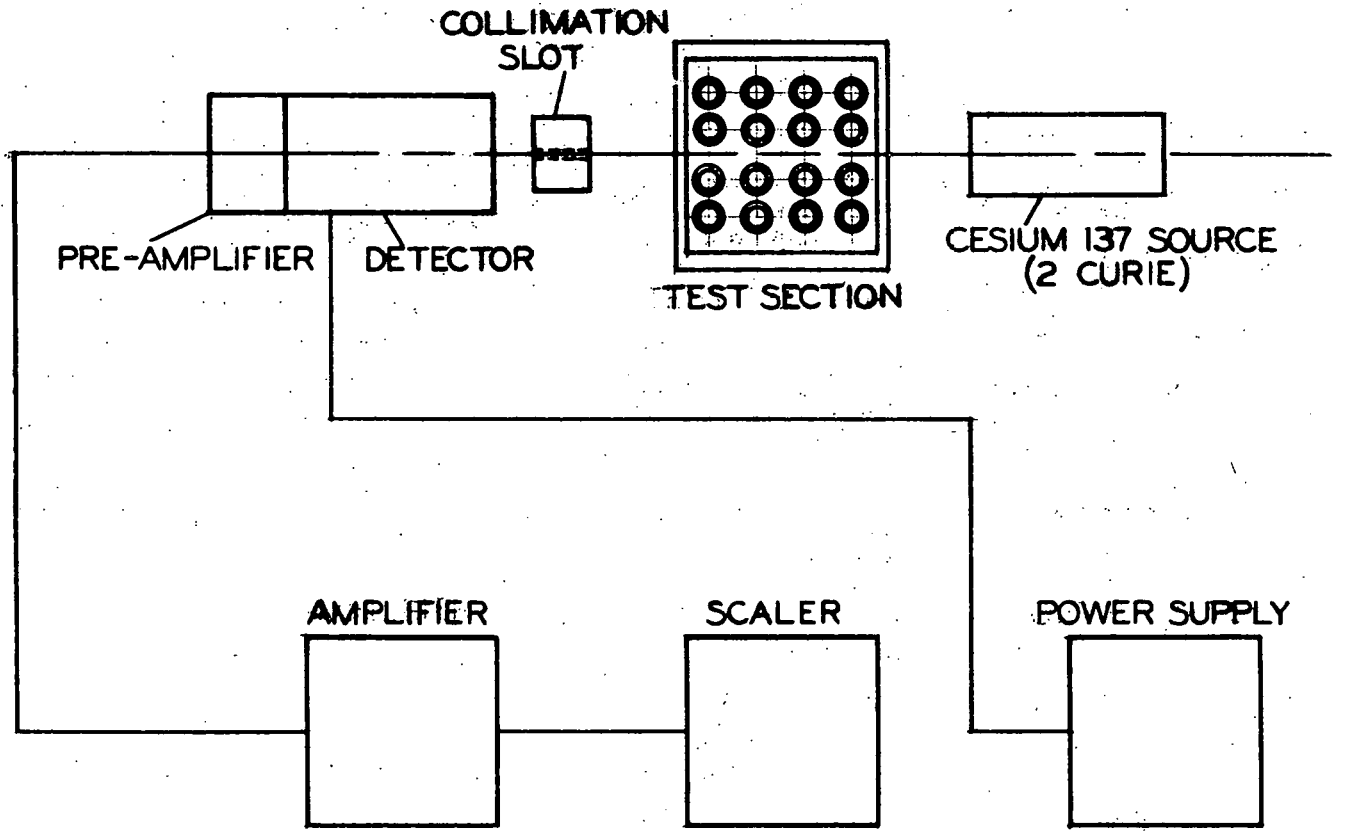

Figure 16 - Gamma Attenuation Equipment Block Diagram (43-024-985)

slot located on the detector side of the test section. The photomultiplier tube detector had a 1.25 in. diameter Sodium Iodide crystal which is located against the collimator slot.

The count rate measured by this system was assumed to be directly proportional to the incident radiation intensity reaching the detector. Thus, the efficiency and calibration of the instrumentation are unimportant so long as only ratios of count rates are used. The assumption of linear proportionality is acceptable so long as the count rate does not exceed the "linear" capacity of the equipment.

Analysis here and elsewhere indicated a sensitivity of void measurements both to small changes in high voltage applied to the various stages of the photomultiplier tube and also to changes in temperature. These effects became very important to the Greendale program since a single traverse of a test section required two hours.

Before and after each traverse, a reference count rate through a 5/8 in. steel plate was obtained. Because of the inherent tendency of the electronic equipment to drift, this reference count varied slightly (about 4 per cent in 2 hr) over a period of time. It was experimentally determined that the assumption of linear drift was valid. Thus all of the data

were adjusted to a common reference before the void fractions were computed.

The entire detector was surrounded by copper cooling coils. The water supply and exhaust temperatures were experimentally found to be essentially constant. The manufacturer's specifications indicated relative insensitivity to changes in incoming line voltage and a $\pm$0.05 per cent long term stability. The incoming line voltage was varied between 100 and 125 volts using a variac and no significant effect on counting rate was observed.

The complexity of the test sections used and the manner of obtaining data made exacting demands on precise and reproducible positioning of the source and detector. Thus, a special rack was designed and built. This rack provides 12 ft of vertical travel and 8 in. of horizontal travel. Horizontal position could be determined and reproduced to within 0.005 in. Test sections up to 10 in. wide can be accommodated between the source and the detector platform. When in use, the rack is jacked up off the floor on four screws to maintain its position.

8.2 Void Measuring Procedure

The void data were taken at two locations: 2 in. downstream from the set of spacers located 18 in. from the test section inlet, and 2 in. upstream from the set of spacers located 54 in. from the test section

inlet. The beam path length available for flow varied from 0.736 in. through the pin rows to 2.4 in. between rows of pins. The corresponding ratios of "empty" to "full" count rate readings varied from about 1.13 to 1.49.

A void measurement was obtained by collecting a series of empty, hot (saturated) water, and two-phase count rates at each fixed position on the test section. A hot water reference and an empty reference consisted of taking a series of count rates at physical locations 0.020 to 0.040 in. apart. Eighty separate count rate readings were recorded for each traverse. In order to determine whether the magnetic field caused by the current flow in the test section had any effect on the radiation measuring system or caused any unusual movement among the rods, a special series of hot water "with power" measurements were obtained. For these measurements, the water temperature was maintained at saturation for 600 psia, the power planned for the two-phase run was applied to the test section, and the system was over pressurized to 700 psia to prevent any boiling. (The hot water "no power" runs were performed in a similar fashion, but no power was applied to the test section.) Once the empty and the hot water references were established, the count rate readings for steam-water mixtures were taken at the same physical locations as were the references for the empty and hot water data.

In order to take into account the change in test section position due to thermal expansion, all the data were plotted on large graph paper and each traverse was aligned so that the pin center positions corresponded to those of the empty run.

8.3 Results

8.3.1 Isothermal Pressure Drops

Before beginning the boiling pressure drop measurements, the test section was operated at isothermal conditions (all liquid with no power). These data were taken over the same range of mass flow rates as were planned for the two-phase tests ($G = 1.0 \times 10^6$ to 2.5×10^6 lb/hr-ft^2). The data were reduced to isothermal friction factors (f_{iso}) for the flow over the rods and form loss coefficients (K_{iso}) for the flow through the spacers.

When plotted versus Reynolds number, the isothermal friction factors exhibited considerable scatter ($\pm$50 per cent). The general magnitude, however, was in agreement with the Moody curve (3). Inspection of the data showed that the data scatter was much smaller ($\pm$20 per cent) when each of the 9 in. lengths were considered separately. It is believed that the varying magnitudes of f_{iso} among the 9 in. lengths resulted because of the sensitivity to tap location when the tap is near a spacer. It is noted that the pressure drops from which the friction factors were calculated were relatively small, varying from 0.1 psi to 0.3 psi.

The primary purpose of the isothermal data was to serve as a reference in calculating two-phase multipliers. Since each length showed a different level, a separate isothermal reference was used for each 9 in. length in reducing the boiling data.

8.3.2 Bulk Boiling Frictional Pressure Drops

After the isothermal friction factors were well established, power was applied to the rods, and boiling pressure drop data were taken. With inlet subcooling held at approximately 0 - 15 Btu/lb, it was possible to achieve exit qualities from 0 - 5 per cent by varying the amounts of test section power and mass flow rate. All tests were conducted with the test section exit pressure held at 600 psig.

In these tests mass velocity (G) was varied from 1.0×10^6 to 2.5×10^6 lb/hr-ft^2 (in the lower half) and up to 360 kw were applied to the test section by the M-G set. These conditions resulted in heat fluxes (ϕ) as high as 150,000 Btu/hr-ft^2 in the lower half and 90,000 Btu/hr-ft^2 in the upper half.

In reducing the data it was necessary to remove the effects of elevation and acceleration in order to isolate only the frictional losses.

These two items were calculated using the following relationships:

$$\Delta P_{ele} = \Delta Z \, \bar{\rho}_{TP} \tag{16}$$

$$\text{where } \rho_{TP} = R_g \rho_g + (1 - R_g) \rho_L \tag{17}$$

$$\Delta P_{accel} = \frac{G^2}{g_c} \left\{ \left[\frac{(1 - X)^2}{1 - R_g} v_f + \frac{X^2}{R_g} v_s \right]_{out} - \left[\frac{(1 - X)^2}{1 - R_g} v_f + \frac{X^2}{R_g} v_s \right]_{in} \right\} \tag{18}$$

The magnitude of these calculated quantities ranged from 25 to 50 per cent of the measured pressure drops. Values of R_g used in these calculations were taken from the homogeneous model. The same calculations were made using Martinelli voids (5), and comparison showed that the differences in the calculated corrections were less than 5 per cent for the low quality range studied. The Martinelli voids yielded slightly larger values for φ_{LO}^2. Hence the values of R_g from the homogeneous model were chosen because of simplicity of calculation.

As noted above, the elevation and acceleration corrections were of the same order of magnitude as the measured values. While this was undesirable from the standpoint of studying friction effects, it was necessarily included in simulating

the Pathfinder operation. It is encouraging to note that even with the use of the simple homogeneous model for these calculations, the friction data from the lower and upper half of the test section are in good agreement even though the relative contribution of elevation and acceleration effects was significantly different in these two regions.

All frictional pressure drops were ultimately reduced to two-phase multipliers (ϕ_{LO}^2). The data are presented in Figure 17 as a function of mass velocity and steam quality (taken at the center of each length increment). Mass velocities shown on the plot are the mass velocities in the lower half of the test section. The upper half mass velocities are 13.6 per cent less than in the lower half. The data represent the top 6 length increments as bulk boiling was not encountered in the lower 2.

Figure 17 also shows the prediction of ϕ_{LO}^2 based upon the Martinelli-Nelson correlation modified by a flow effect (8 and 9). The agreement of the data with the prediction is generally within $\pm$25 per cent. The original Martinelli-Nelson correlation (5) allowed for no flow effects, and it would approximately correspond to the $G = 1.25 \times 10^6$ line. The agreement of the data with this line is not perceptibly worse than $\pm$25 per cent; however, some effect of flow is evident. For the particular set of conditions studied, the

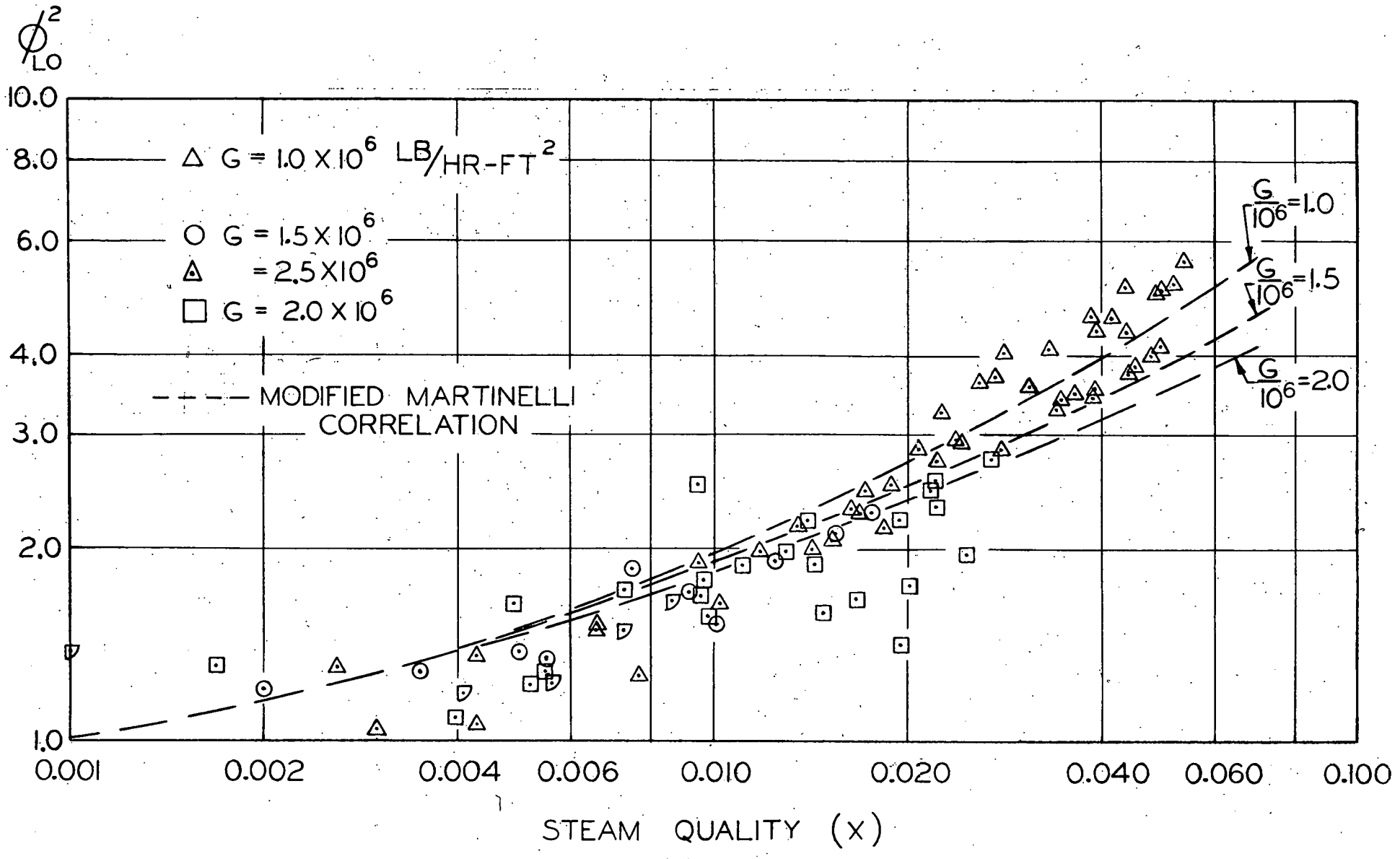

Figure 17 - Boiling Friction Losses as a Function of Quality and Mass Velocity

(43-024-774)

Isbin correlation (6) is in close agreement with the modified Martinelli relationship (8 and 9). The Isbin ϕ_{LO}^2 vs. quality lines, at constant flow, have a smaller slope than the curves shown in Figure 17, and do not appear to be curving upward as fast as the data at the higher qualities.

It was concluded that the modified Martinelli (8 and 9), the Martinelli-Nelson (5), and the Isbin (6) correlations all describe the data within about $\pm$25 per cent for the range of conditions studied. While the data do exhibit some flow dependency, it is impossible to define the extent and nature of this dependency from the present experiments.

8.3.3 Bulk Boiling Form Pressure Drops

Form loss coefficients (k) were calculated for each spacer and also for the inlet and exit losses. Since there was no significant boiling occurring at the inlet or spacer 1 (numbering from the bottom up) the discussion of boiling effects on form losses will be confined to spacers 2 and 3 and the exit.

Spacer 3 represented a simple form loss, and the two-phase loss coefficient was initially reduced from the data by the equation:

$$\frac{k}{\Sigma^2} = \frac{P_{meas}}{G^2/2g_c\ \rho_f} \qquad (19)$$

Spacer 2 and the exit section included net flow area expansions so that the calculation of loss coefficients in these regions was more complicated. The general equation used was:

$$\frac{k}{\Sigma^2} \quad \frac{P_{unrec}}{G^2/2g_c\ \rho_f} \quad \frac{P_{meas} - P_{rec}}{G^2/2g_c\ \rho_f} \tag{20}$$

Evaluating the recoverable pressure drop (ΔP_{rec}) to use in this equation is difficult. Two different approaches were taken to calculate this quantity.

The first assumes that the fluid can be considered to behave as if it were homogeneous with a density equal to the average density of the two phases. Then,

$$\Delta P_{rec} = \frac{G^2}{2g_c\ \bar{\rho}_{TP}}(\sigma^2 - 1) \tag{21}$$

where σ is the area ratio of the expansion (as in Eq. 7 and 8).

Using this procedure and Equation 20, the unrecoverable loss coefficients (k_1) were calculated. These loss coefficients were then compared with the isothermal loss coefficients and the results are plotted in Figure 18. The procedure of using $\bar{\rho}_{TP}$ to account for the two-phase effects in the unrecoverable component was examined (Eq. 7).

This would be valid (i.e. - Eq. 7 would be accurate) if

$$\frac{k_l}{k_{iso}} = \frac{\rho_f}{\overline{\rho}_{TP}}$$

However, the agreement shown in Figure 18 is not good, and the points are generally higher than the ρ_f/ρ_{TP} line. For spacer 2 and exit, the points are closer to the φ_{LO}^2 correlation. See Equation 8.

The second approach used was to assume, as Lottes did (10), that all the pressure recovery is due to the liquid phase expansion (Eq. 9). This results in an expression of the form:

$$\Delta P_{rec} = \frac{G^2}{2g_c \rho_f (1 - R_g)^2} \qquad (22)$$

Using these results and Equation 20, the calculated k's are higher than with Equation 21 for spacer 2 and the exit. These points are plotted in Figure 19 and compared to a line which represents Equation 9, $k/k_{iso} = 1/(1 - R_g)^2$. The agreement is good for spacer 2 and the exit but not for spacer 3.

A third alternative for handling the form losses with net area changes is to use Equation 19 and calculate a combined k. Following this procedure to calculate the k's for all three stations gives the results shown in Figure 20. The

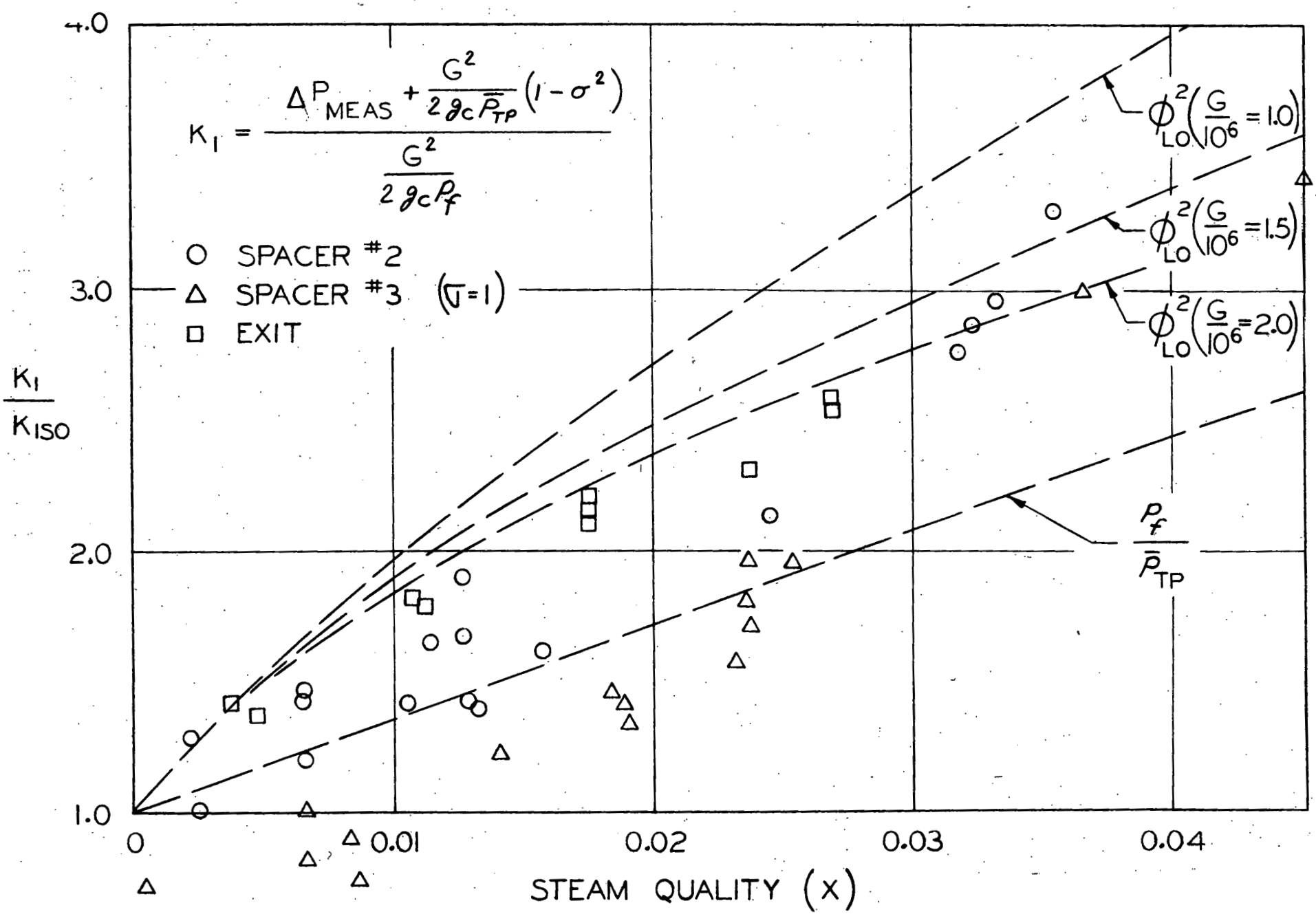

Figure 18 - Boiling Effect on Form Loss Coefficient (43-024-771)

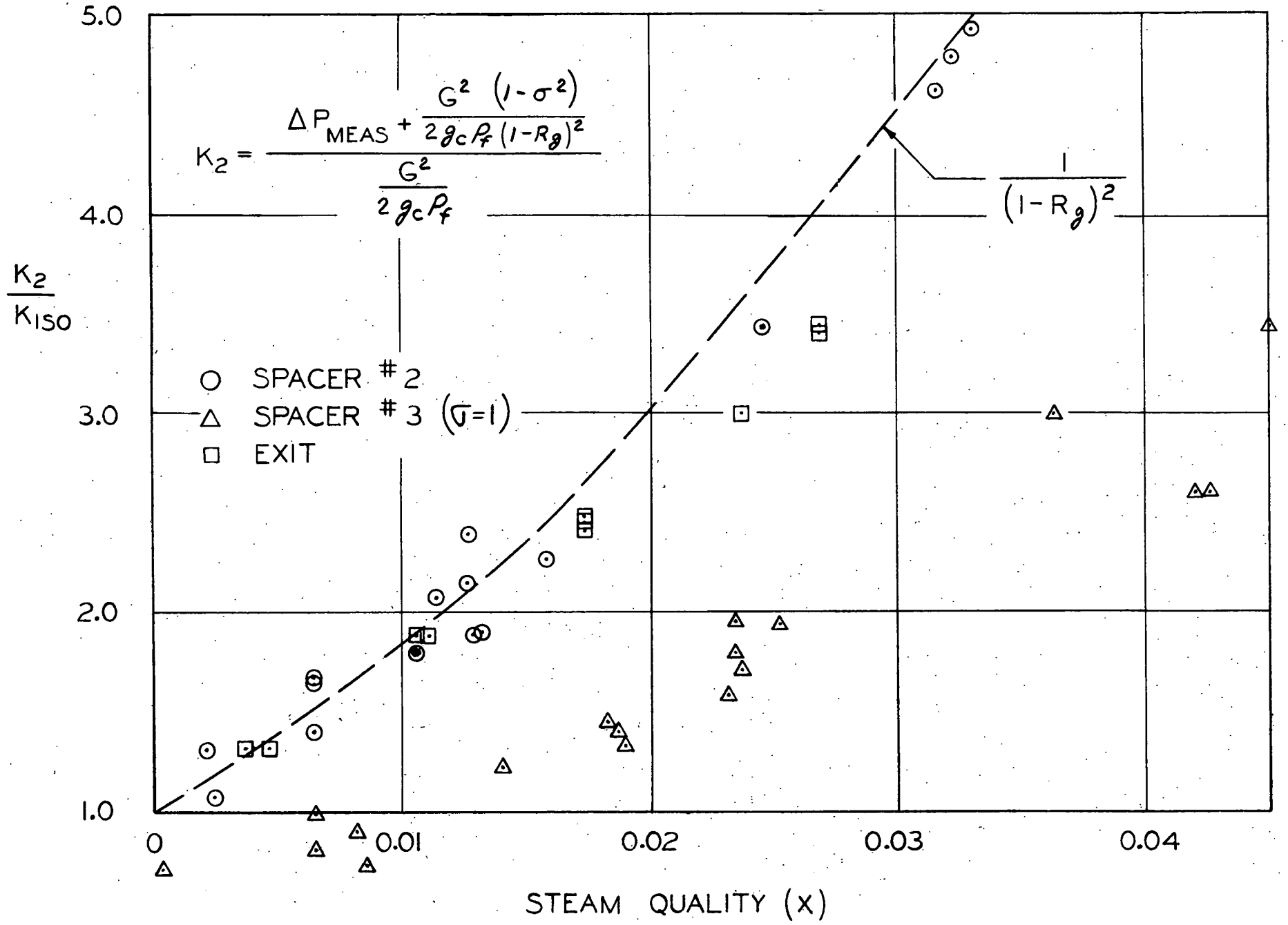

Figure 19 - Boiling Effect on Form Loss Coefficient (43-024-772)

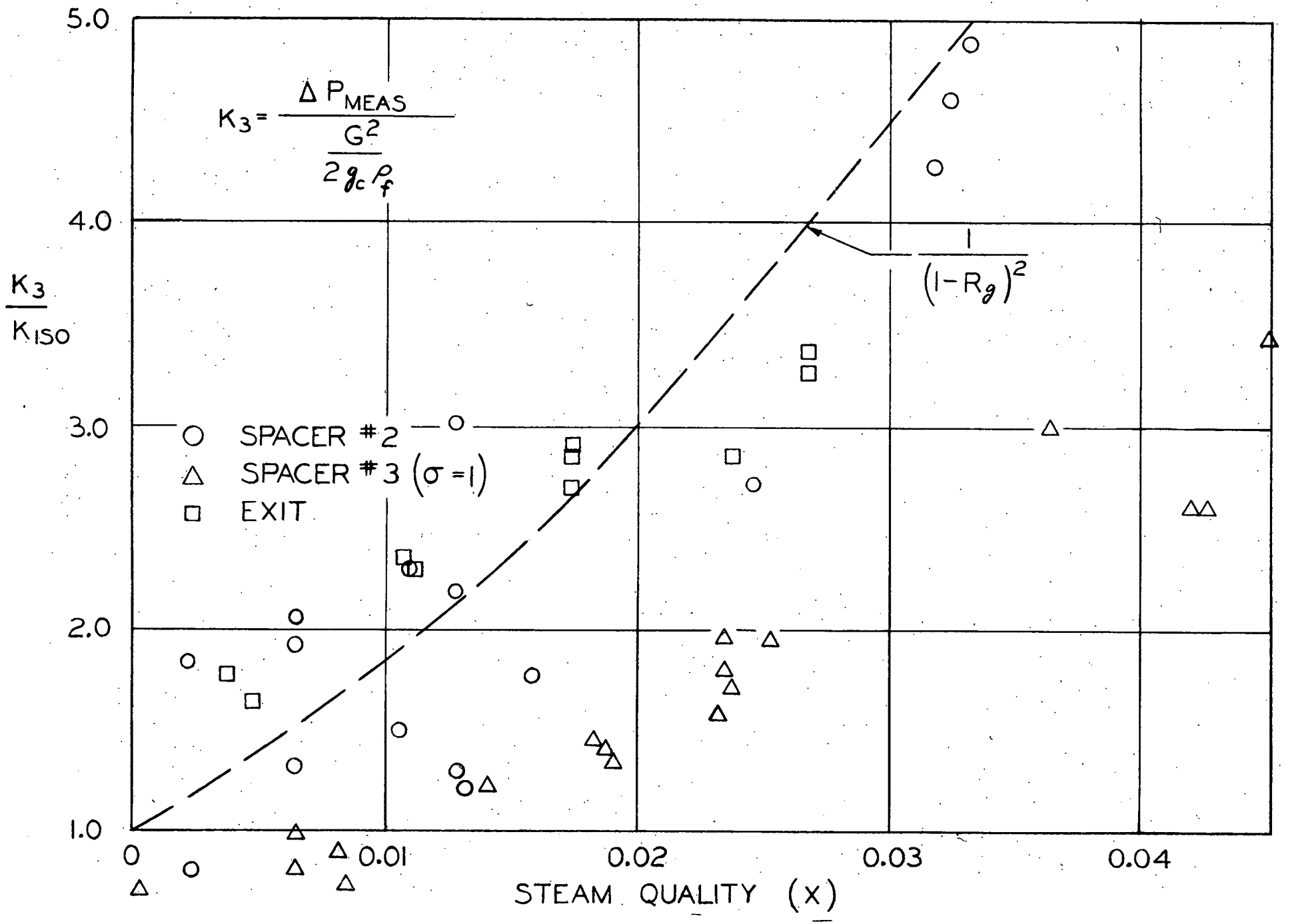

Figure 20 - Boiling Effect on Form Loss Coefficient (43-024-773)

ratios of two-phase to single-phase loss coefficients are again compared with the Lottes model with fair agreement. It is noted that the comparisons shown in Figures 19 and 20 are really showing pressure recovery in different ways. The accuracy of the Lottes type model is better assessed from Figure 20.

The data from spacer 3 are disturbing in that the two-phase losses appear lower than the single-phase losses at low steam qualities. It is suspected that the original determination of the single-phase coefficient was faulty although an unfortunate test section failure prevented checking this possibility. The suspicion prevents formulation of firm conclusions concerning the pressure losses in this region.

It was concluded that the two-phase form losses are fairly well predicted by the Lottes type model (10). Insufficient data were obtained to permit formulating any new relationships.

8.3.4 Local Boiling Pressure Drops

When friction data from the boiling runs were compared with the isothermal data, it was noted that the losses were significantly higher than the isothermal case just upstream from the location of zero quality (as calculated from the

first low). It is believed that this is due to subcooled nucleate boiling phenomena. In calculating the elevation and acceleration pressure drops, account was taken of the voids in the bulk boiling region but not in the local boiling region.

An attempt to correlate the data was made by using an equation of the form:

$$\frac{f}{f_{iso}} = 1 + \left(\frac{T_{bulk} - T_{lb}}{T_{sat} - T_{lb}}\right) F \qquad (23)$$

where $T_{lb} = T_{sat} + \Delta T_{J\&L} - \phi/h$

The local boiling temperature (T_{lb}) is the lowest bulk temperature at which local boiling will begin according to the Jens & Lottes correlation (24). The Jens & Lottes correlation is given by:

$$\Delta T_{J\&L} = 60\ (\phi/10^6)^{0.25}\ e^{P/900} \qquad (24)$$

where ϕ is the heat flux in Btu/hr-ft^2 and P is pressure in psi.

To determine the factor F in Equation 23, the data were plotted with $\left[f/f_{iso} - 1\right]$ as an ordinate versus $\frac{T_{bulk} - T_{lb}}{T_{sat} - T_{lb}}$ and this plot is shown in Figure 21. The scatter was found to be quite large ($\pm$50 per cent). However,

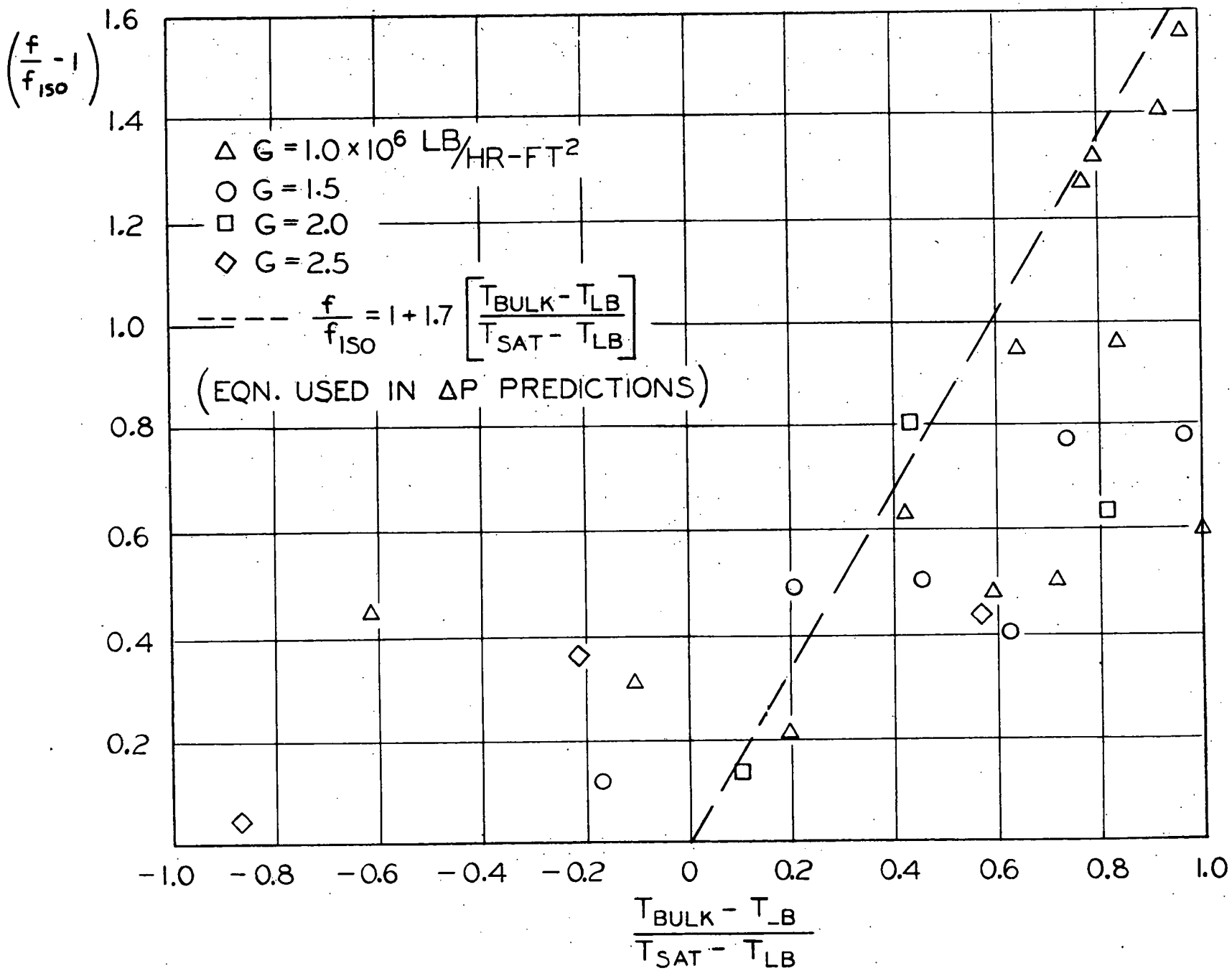

Figure 21 - Effect of Local Boiling on Friction Factors (43-024-775)

a trend was present and a line with a slope of 1.7 (i.e., F = 1.7) will yield conservative pressure drop results.

8.3.5 Over-all Pressure Drops

To test the multiplier method of predicting the boiling pressure drops, calculations were made to predict the over-all pressure drop (excluding the entrance and exit) from the available correlations. The frictional losses were calculated from the Moody friction factor, the modified Martinelli correlation for ϕ_{LO}^2, and Equation 23 for local boiling. Form losses were determined from the measured isothermal values and Equation 9.

The following table gives typical comparisons of calculated and measured values along with the test conditions.

OVER-ALL PRESSURE DROP COMPARISONS

P Calculated	P Measured	Per Cent Deviation	G	Exit Quality
5.13 psi	5.16 psi	-0.6	2.18×10^6 lb/hr-ft^2	1.74%
5.50	4.87	+12.9	2.08	2.43
6.04	5.41	+11.6	2.08	2.92

The tabulated comparisons reflect the improved ability to predict results with respect to over-all pressure drop as compared to the separate friction and form type components.

8.3.6 Void Fraction

Following completion of the pressure drop experiments, the void fraction tests were begun. Because these tests were so time consuming and tedious to perform, only five different complete runs (sets of traverses) were completed. Two sets of traverses were carried out at the lower measuring position (see Procedure Section) with mass velocities of 2.18×10^6 and 1.23×10^6 lb/hr-ft^2; and qualities of 0.0053 and 0.0082 respectively. Three sets of traverses were carried out at the upper measuring position with mass velocities of 1.92×10^6, 1.06×10^6, and 1.08×10^6 lb/hr-ft^2, and qualities of 0.0163, 0.0208, and 0.0354 respectively.

As described earlier, each set of traverses included a series of measurements with the test section empty, full of saturated water with no power, full of saturated water at the test power, and containing the two-phase mixture of interest. The measured count rates comprising each traverse were plotted versus horizontal position, and the curves were shifted slightly horizontally to correct for minor mis-alignment (the largest shift was 0.060 in.). This shifting was not due to the inability to reposition the rack, but rather because of uncontrolled movement of the loop piping.

The count rates for the hot water "with power" case were slightly different from the hot water "no power" case and this was attributed to a minor effect of the magnetic field penetrating the photo tube shielding. It was assumed that the field would affect the two-phase results in the same manner, so the values for N_L in the numerator of Equation 14a were taken from the "with power" traverses and the values for N_L in the denominator were taken from the "no power" traverses. In many cases the "with power" and "no power" water count rates differed imperceptibly while in no case did the difference exceed 3 per cent.

Following this final alignment and adjustment of the data, local void fractions were computed from Equation 14a for each horizontal position at which count rates were measured. These local void fractions were plotted as a function of horizontal displacement from the centerline of the nearest row of pins. When viewed in this fashion, the data exhibited an appreciable amount of scatter; some of which was believed to be "honest" scatter, but some of which was believed to reflect real differences among the different regions in the rod array. This method of illustrating the data is shown for a typical run in Figures 22, 23 and 24. Data representing the central region of the bundle, including regions adjacent to the centerlines of the two center-most pin rows, are shown in Figure 22. The solid line represents a mean curve through

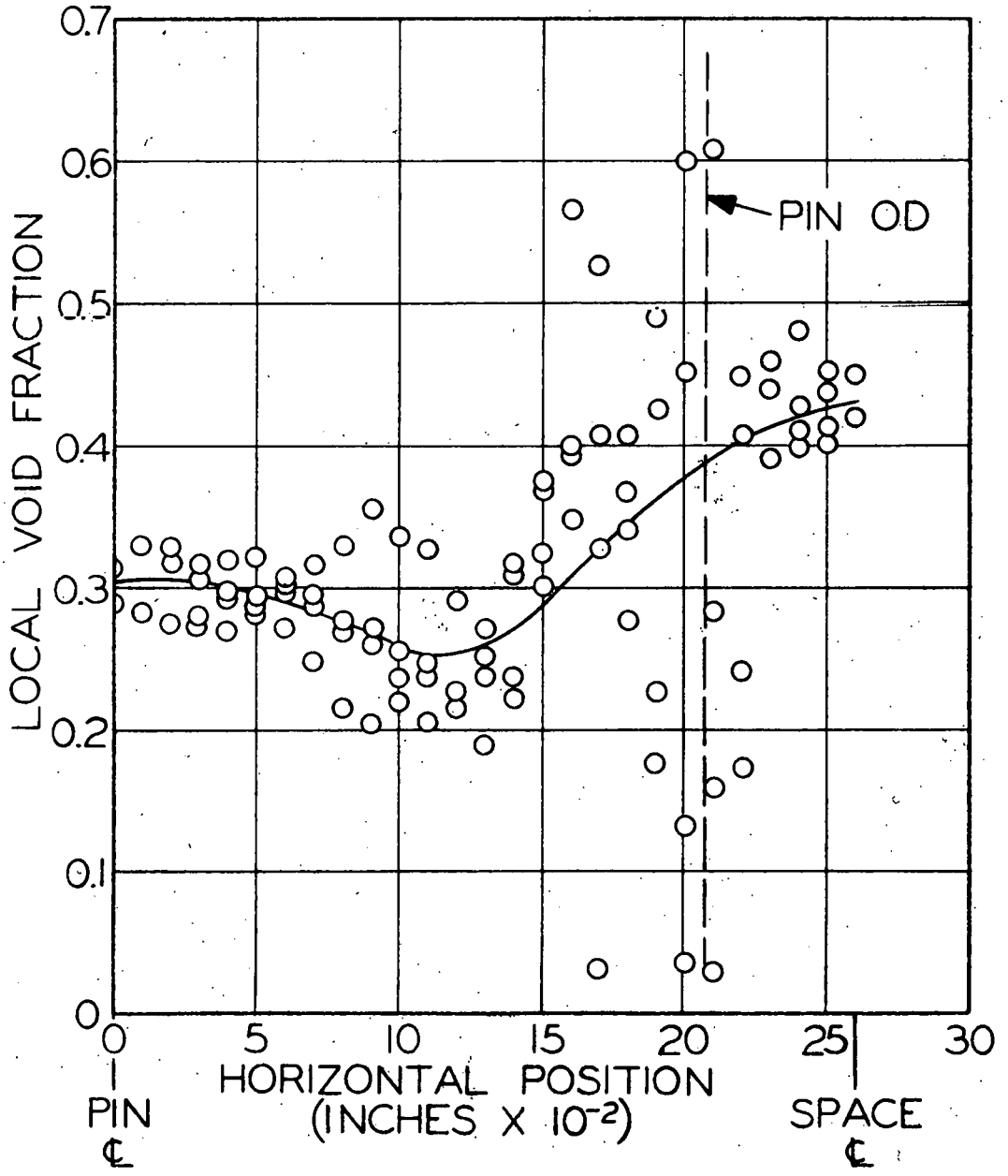

Figure 22 - Local Void Fraction Data Pin Row Centerline to Position Equidistant Between Pin Rows - Data Superimposed 16 Pin Tests (Typical) (43-025-027)

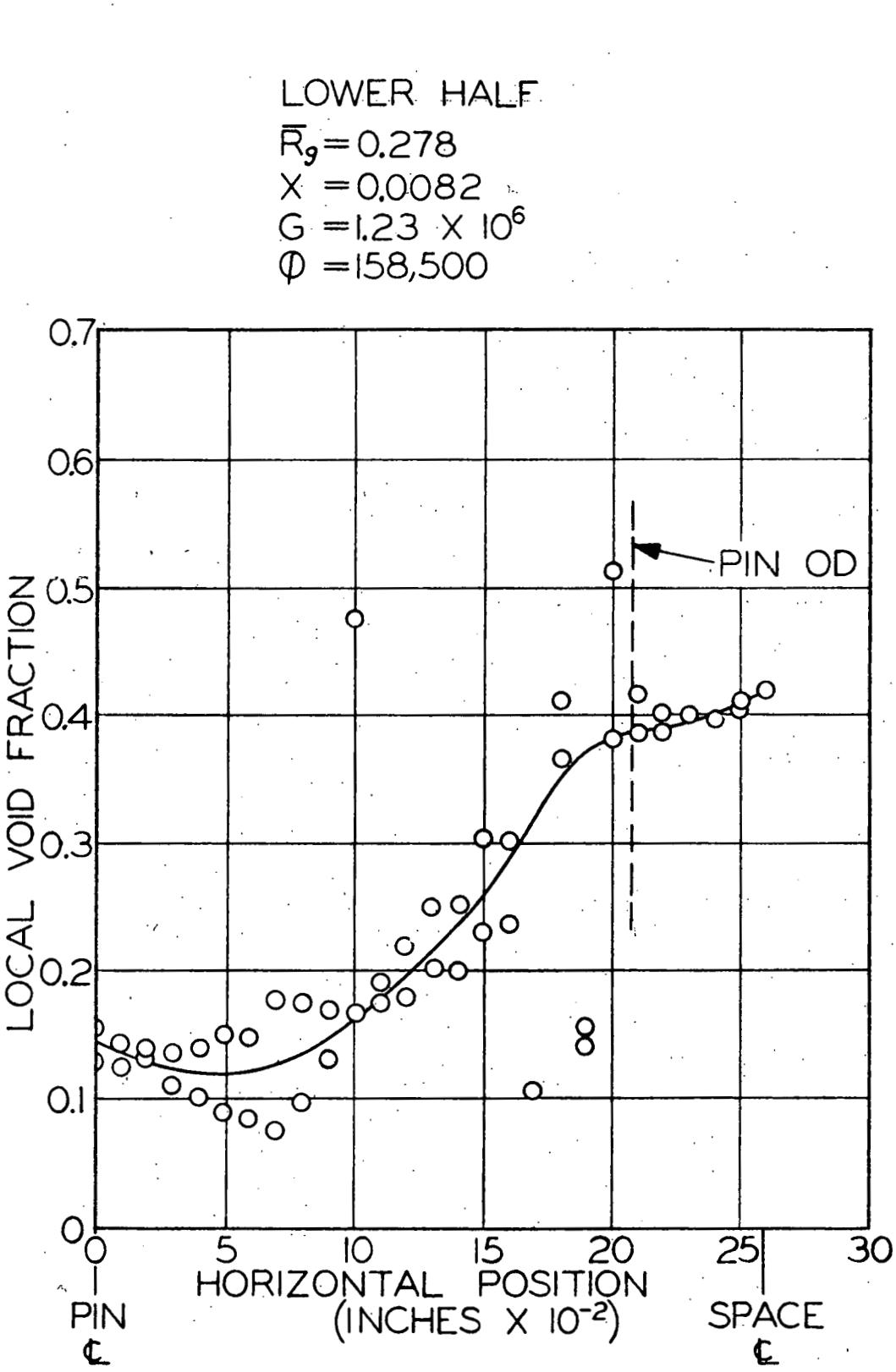

Figure 23 - Local Void Fraction Data Outermost Pin Row Centerline to Position Equidistant Between Pin Rows - Data Superimposed 16 Pin Tests (43-025-028)

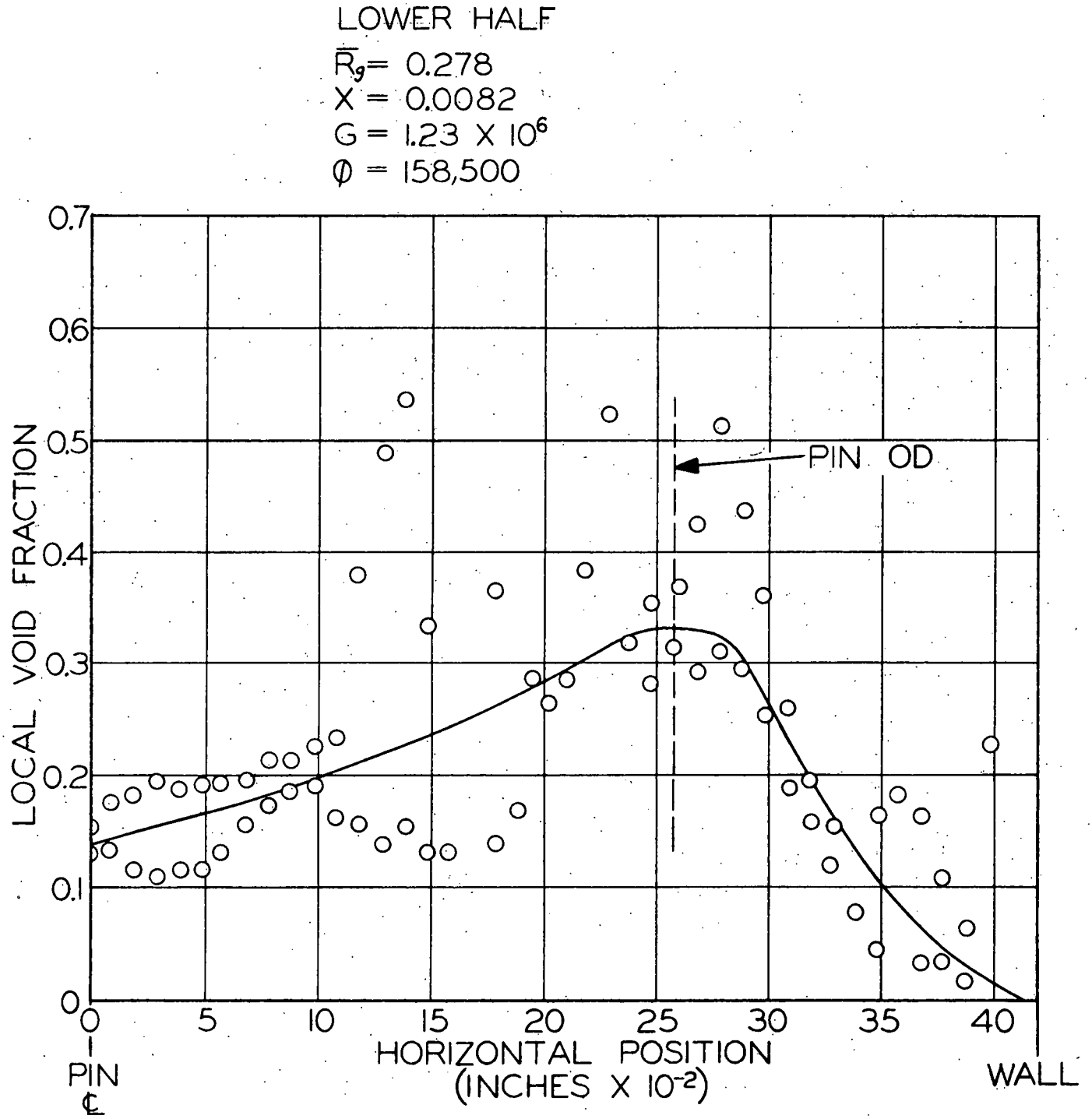

Figure 24 - Local Void Fraction Data Centerline of Outermost Pin Row to Box Wall - Data Superimposed (Typical) (43-025-029

the data. Figure 23 shows the data representing the region just inside the outer-most pin rows, and these data appear to be distinctly different from those shown in Figure 22. Finally Figure 24 shows the data representing the region adjacent to the inner walls of the box enclosure, and these data appear to be different from the data shown in either Figure 22 or 23. While no attempt was made to distinguish among the four center-most regions shown in Figure 22, the complete traverse shown in Figure 28 indicates a slight tendency of the voids to be highest at the center of the bundle.

Curves corresponding to the solid lines in Figures 22, 23 and 24 are shown in Figures 25, 26 and 27 for all five runs. Figure 25 shows the data for the central region of the bundle. The lowest quality studied gave no measurable void fraction in the small gaps between pins and a monotonic increase in void as the spaces between pin rows are approached. The dip in the void fraction curve for the data shown in Figure 22 is seen to occur at about half the pin radius whereas the the dip for the measurements in the upper half of the bundle occurs just outside the pin radius. This may be due to the fact that the data for the lower half were obtained just downstream from a spacer while the data for the upper half were obtained just upstream from a spacer. Thus, the upper half data may be more representative of a better established

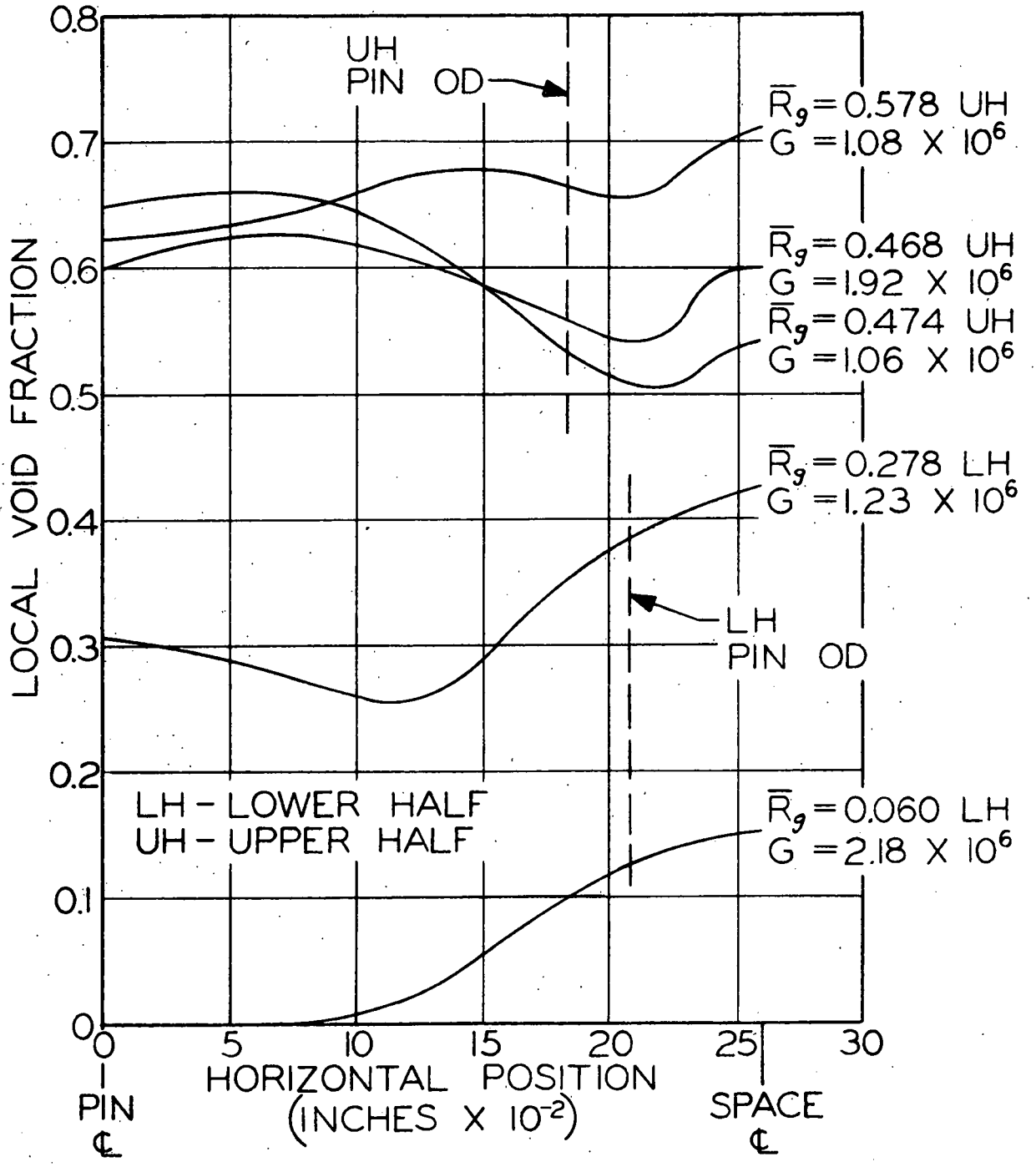

Figure 25 - Local Void Fraction Distribution (Mean Curves from Superposition Averaging) Pin Row Centerline to Position 16 Pin Test (43-025-025)

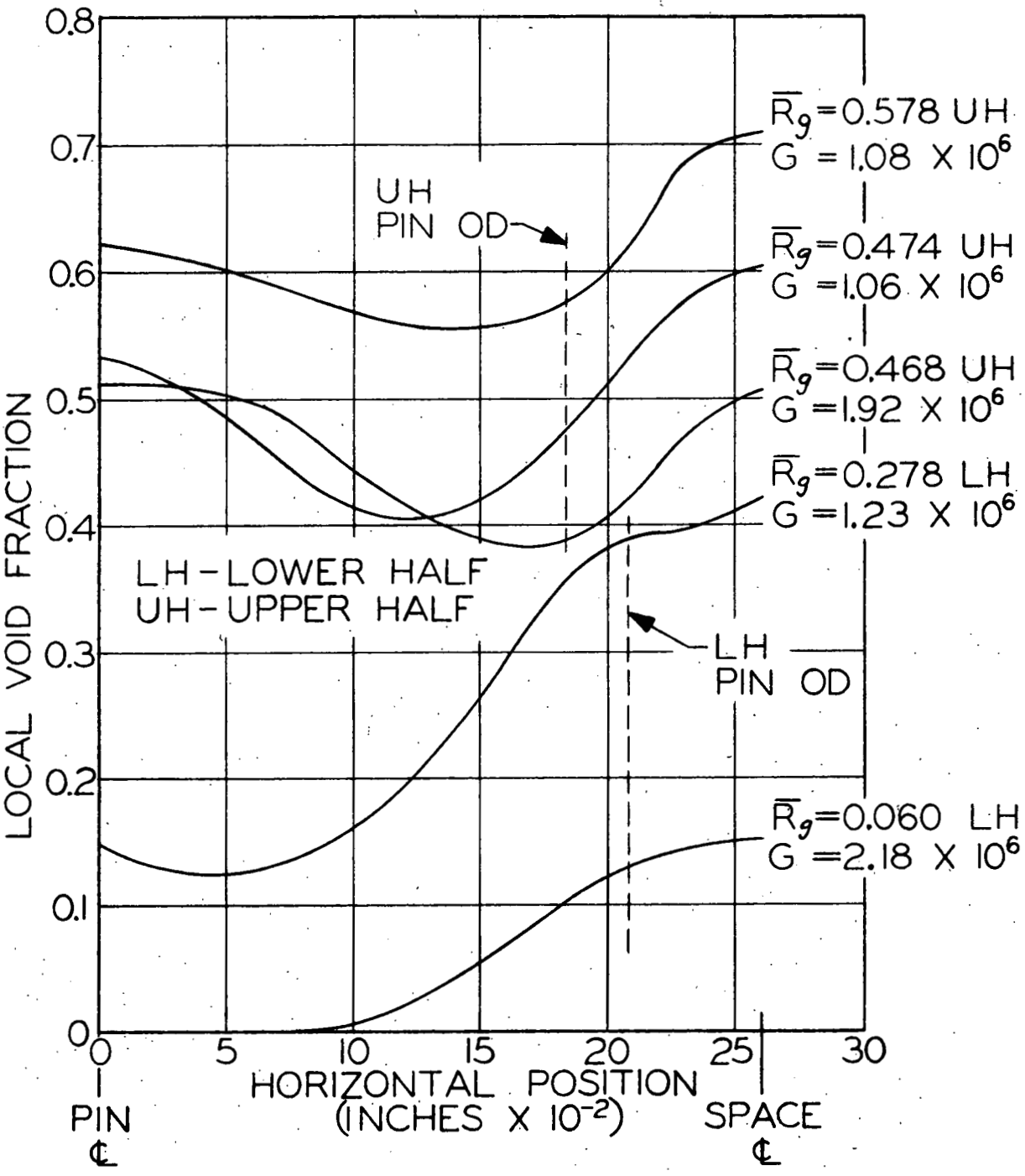

Figure 26 - Local Void Fraction Distribution (Mean Curves from Superposition Averaging) Outermost Pin Row Centerline to Position Equidistant between Pin Rows 16 Pin Tests (43-025-024)

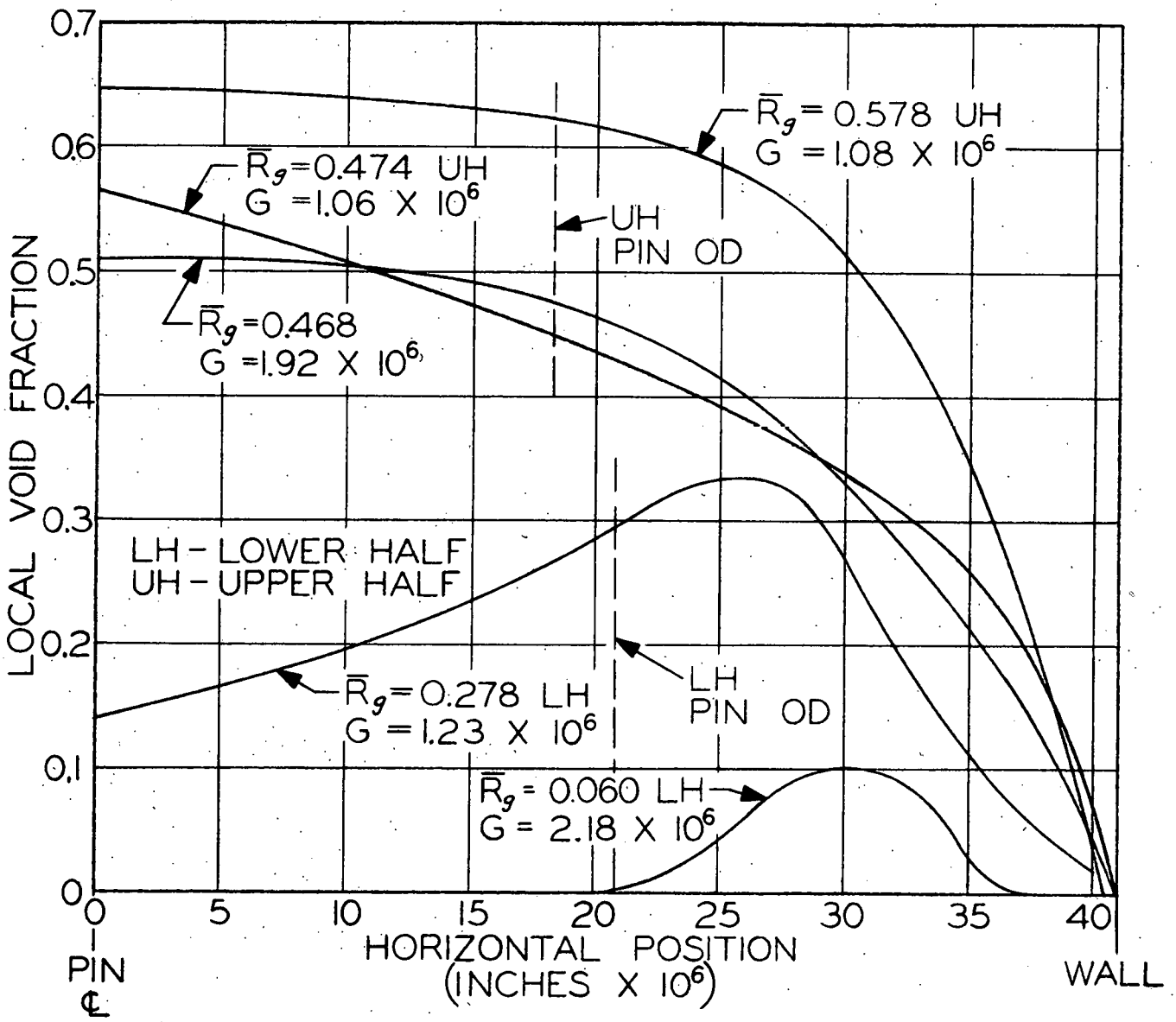

Figure 27 - Local Void Fraction Distribution (Mean Curves from Superposition Averaging) Centerline of Outermost Pin Row to Box Wall 16 Pin Tests (43-025-026)

flow pattern. It is also interesting to note that while the "space" void fraction increased from 0.58 to 0.71 as the quality increased from 0.0208 to 0.0354, the void fraction in the small gaps between pins did not increase appreciably (the flow was nearly the same). This may imply a tendency for the void fraction to reach a "limiting" value in the small gaps with further increases tending to come at the expense of the space between pins.

Data for the region just inside the outer-most row of pins are shown in Figure 26. In this region, the curves for the lower half runs indicate no appreciable dip in void fraction, whereas the upper half data shows a dip just beyond half a pin radius from the pin centerline.

Finally the data for the region near the inner wall are shown in Figure 27. In all cases, the void fraction goes to zero at the wall with the data from the lower half of the bundle exhibiting a peak outside the pin radius, with no such peaking appearing in the data from the upper half. This may be a manifestation of the tendency of the spacers to force the vapor to the outside of the bundle; although there is no such effect apparent from the spacer geometry. Nevertheless, the effect may be produced by the spacer resistance to flow evening out the vapor distribution and acting as a diffuser.

The data shown in Figure 28 are typical of the other four runs with respect to the general shape of the void distribution. The data clearly indicate that the void fraction goes to zero at the inner unheated walls of the enclosure, and this is not surprising. The data also indicate a strong tendency for the vapor to collect in the regions between pins, and this is in agreement with the results reported in (22) for an unheated, air-water system. The void distribution in the small gaps between pins appears to be different in the center of the array than it is in the outer pin rows. It is noted that the void distribution shown in Figure 28 is not truly two-dimensional since each point represents a mean value along the measurement path. A more lucid explanation of the physical significance of the shape of this distribution must await the completion of a parallel analytical study in which various two-dimensional distributions will be postulated attempting to find one which would look like the curve in Figure 28 when viewed in one dimension.

It is also apparent from Figure 28 that the assumption of a uniform void distribution in the reactor neutron diffusion and/or cell calculations may be unrealistic (and even non-conservative when the array is bordered by a control rod water channel). Furthermore, it is likely that the description of the void distribution in a rod bundle with a non-uniform

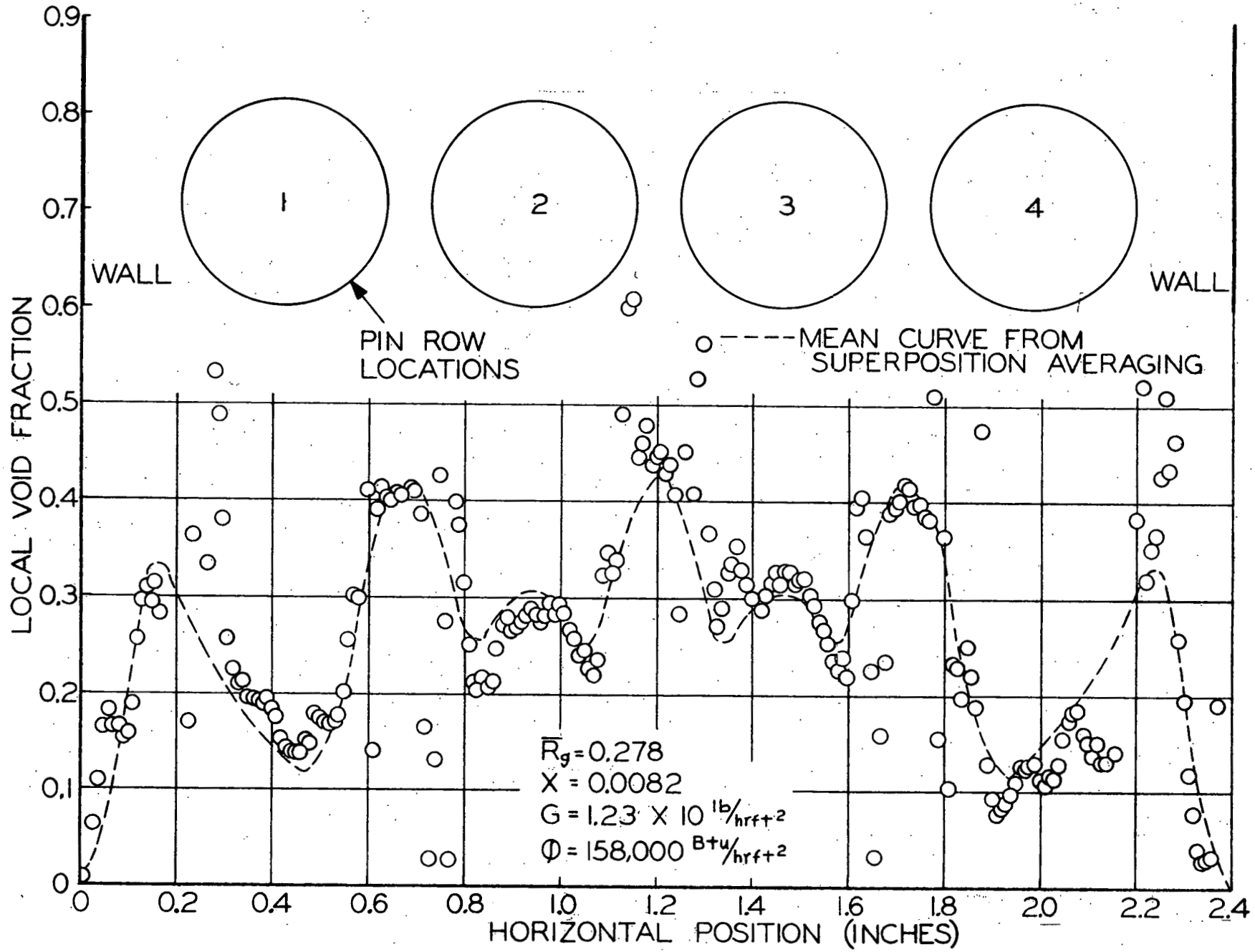

Figure 28 - Local Void Fraction Distribution Vertical Upflow 600 PSI 16 Pin Tests

(45-025-021)

radial power distribution may be appreciably more complicated than previously expected since the distribution in a bundle with a uniform radial power distribution is already quite intricate.

The gross radial void distribution for the five runs is shown in Figure 29. In this representation, each point represents a mean value of the void fraction over a region bounded by the centerline of a row of pins and the box wall or the plane equidistant between pin rows. The tendency of the void fraction to reach a maximum at the center of the bundle, as seen in Figure 28, is not inconsistent with the general shape of the curves in Figure 29 (which were forced to be flat in the center by the data reduction technique). Again the tendency of the gross void distribution to be more uniform just downstream from a spacer than exists just upstream from a spacer is apparent.

The over-all integrated void fractions for the five runs are shown in Figure 30 and compared to existing models and correlations. The data appears to indicate appreciable scatter; however, in light of the complicated nature of the distributions within the bundle, this is difficult to assess. It is noted that the uncertainty in the quality calculation is not negligible--an error in inlet temperature of 1 F would cause an error in quality of 0.0016. It is felt that the

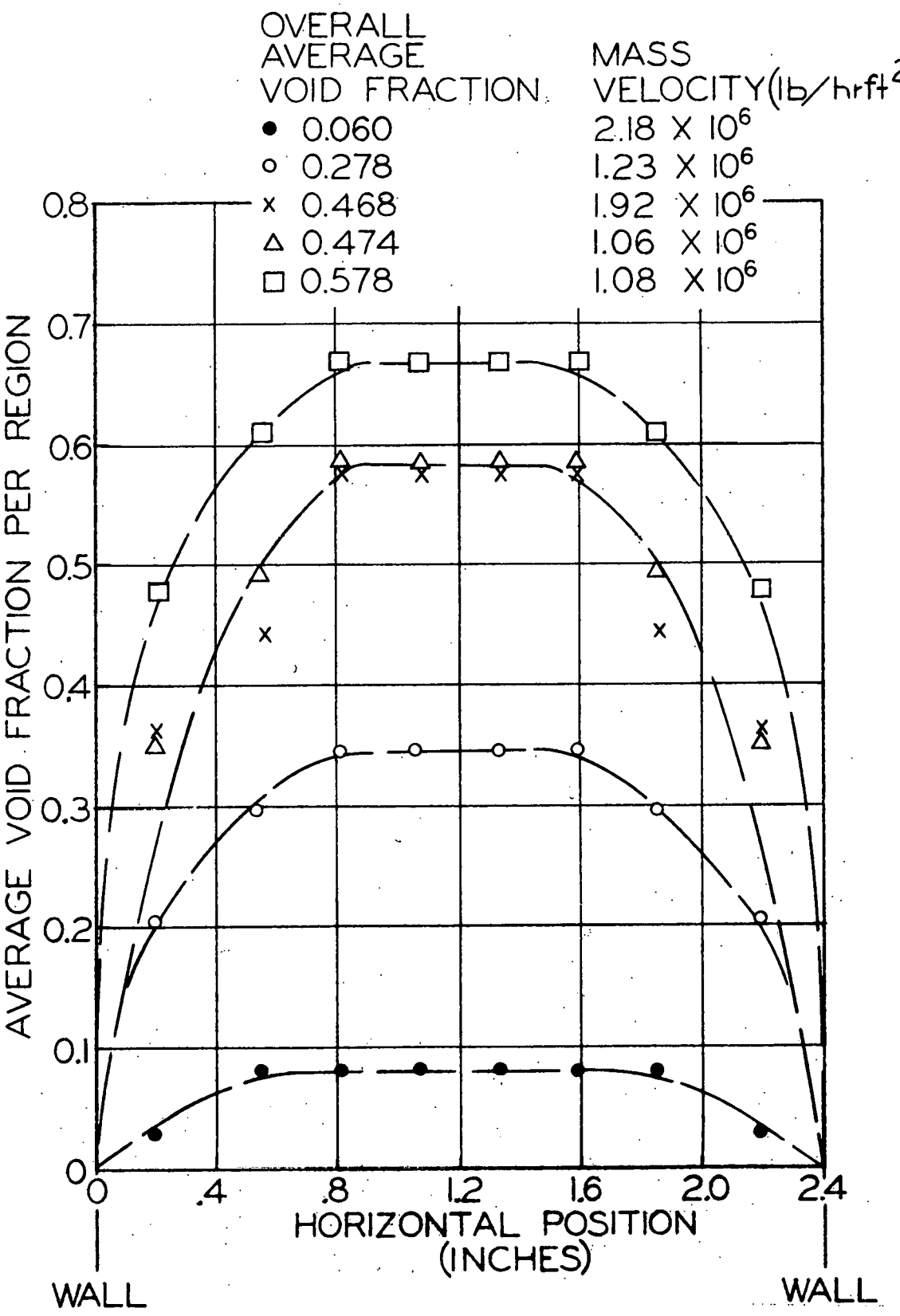

Figure 29 - Gross Region - Wise Void Distributions Vertical Upflow 600 PSI 16 Pin Tests (45-025-022)

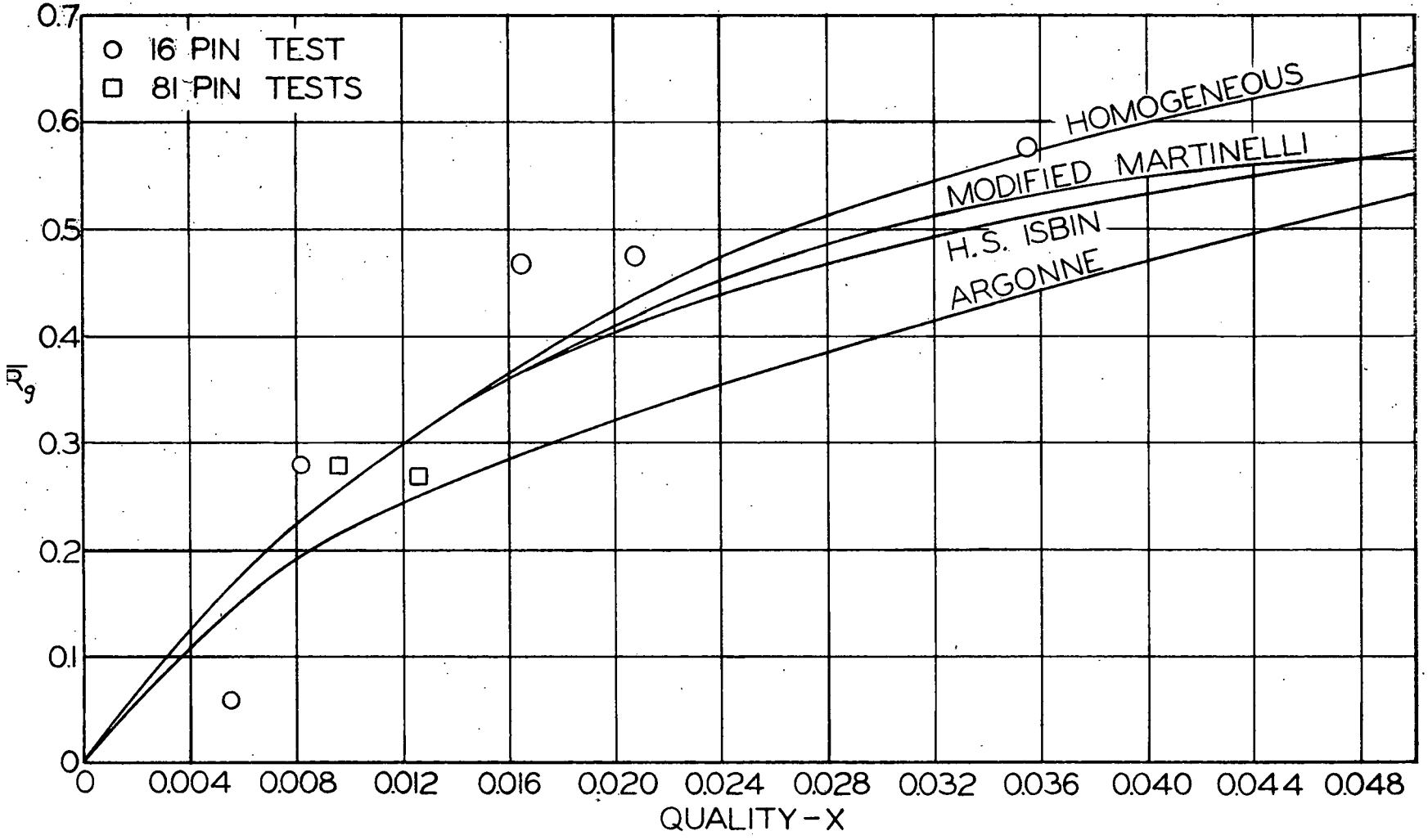

Figure 30 - Over-all Mean Steam-Water Void Fraction ($\overline{R}g$) 600 PSIA (43-025-023)

data tend to support the homogeneous model more strongly than any of the other three relations illustrated.

8.4 Conclusions

1. The two-phase multipliers for boiling at 600 psi are described by the Modified Martinelli relationship (8 and 9) to within ±25 per cent.
2. The two-phase steam-water form loss multipliers are described by the Lottes model (10) to within about ±30 per cent (not considering the data for spacer 3).
3. The void distribution within the rod bundle is non-uniform with vapor collecting in the spaces between pins and liquid collecting in the spaces between pins and liquid collecting adjacent to the unheated enclosure walls.
4. Accurate predictions of the void and power distribution within a parallel rod type boiling nuclear fuel element cannot be achieved until the void distribution for a uniform (radial) power distribution is further investigated.
5. The over-all integrated void fraction in the bundle cross section was found to be reasonably consistent with the homogeneous model.

9.0 EFFECTS OF ARRAY SIZE ON BOILING PHENOMENON

9.1 Description of Test Section

To check the effect of array size on the pressure drop and void fraction distributions measured in the 4 x 4 array test section,

a 9 x 9 array test section was constructed and tested in the heat transfer loop. This test section was 6 ft long, and had the same rod sizes, spacing devices, and end connections as were used in the 4 x 4 test section. The containment box was 5 in. square in inside dimension.

The only notable difference between the two test sections, other than array size, was that the pitch was 0.570 in. on the 4 x 4 and 0.535 on the 9 x 9. This was done primarily to hold the equivalent diameters nearly the same on both test sections. The actual equivalent diameter of the 9 x 9 test section was 0.456 in. compared to 0.470 in. for the 4 x 4 test section (calculated for the bottom half of each).

The experiments were performed in the same system as the 16 pin section using similar experimental techniques. The 81 pin section was instrumented for pressure drop at the same axial positions as in the smaller section. However, void measurements were obtained only at the upper position, i.e. - just upstream from the upper spacer.

The larger test section was powered by the Allis-Chalmers unipolar generator having a capacity of 60,000 amp at 30 v. Power levels as high as 1.7 mw were utilized.

9.2 Results and Conclusions

Although the test program on the 9 x 9 array was not so extensive as the 4 x 4 test program, enough data were obtained to demonstrate that the large increase in array size did not appreciably affect the pressure drop or void distribution (i.e. - the same equivalent diameter concept used to analyze the 4 x 4 test section was used for the 9 x 9 array).

The pressure drop comparison is best illustrated by looking at the two-phase friction multipliers (ϕ_{LO}^2) for the 9 x 9 array as shown in Figure 31. As in the case of the 4 x 4 array the data are correlated by the modified Martinelli relationships (8 and 9). It is apparent that there is more scatter present in these data (due to some slight pressure tap burrs), but the mean values are still well described by the modified Martinelli lines.

The void measurements in the 81 pin test section were carried out in a manner identical to that described for the 16 pin section. One of the objectives of these tests was to determine whether there were any differences between the void distributions in the two array sizes. Interest in this area is further stimulated by the curves in Figures 28 and 29 and the question as to the effect of the larger array. Unfortunately, the 81 pin tests were actually performed before the 16 pin tests, and before the experimental technique had been thoroughly refined. The two over-all average void points are included in Figure 30, but it has not been possible

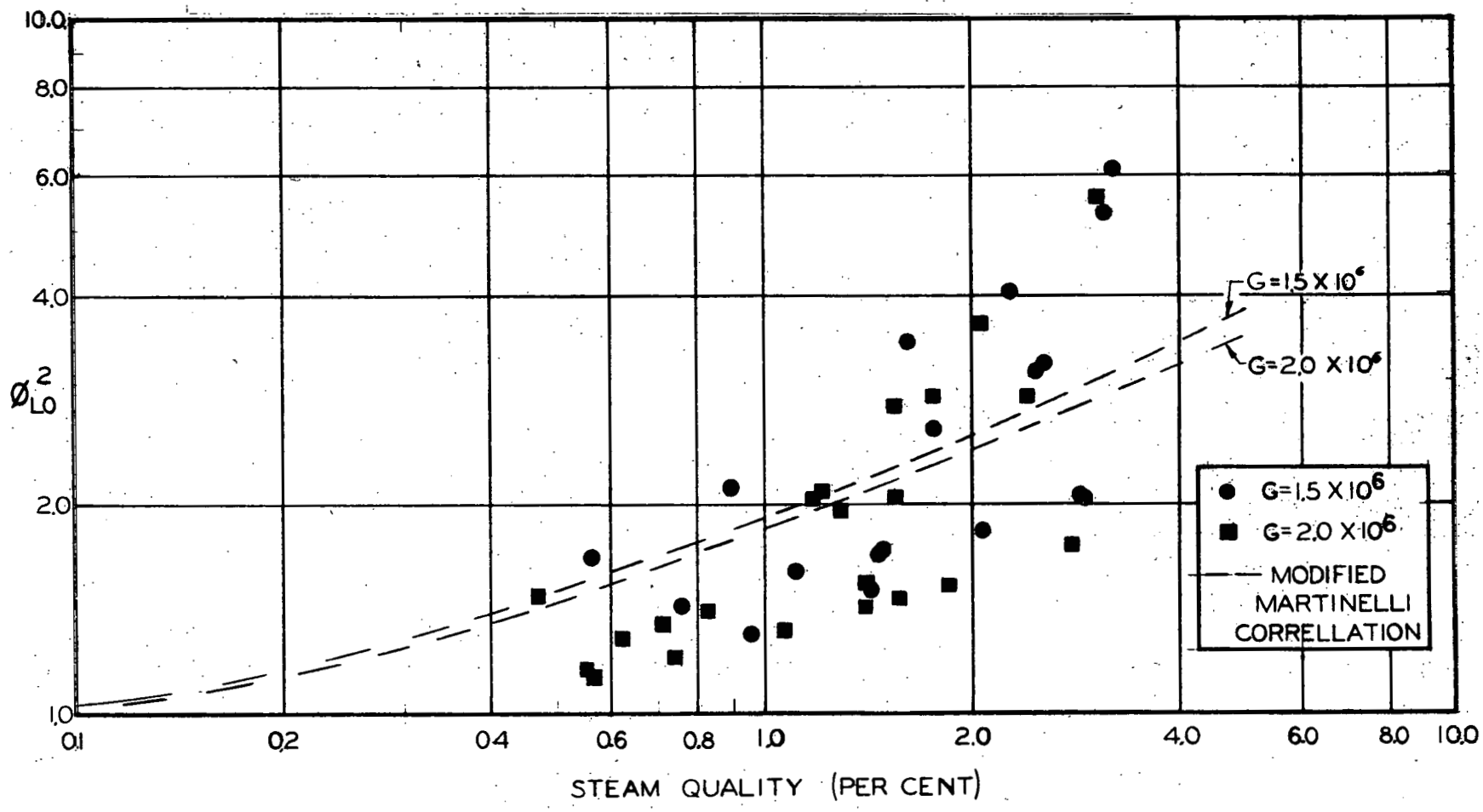

Figure 31 - Two-Phase Frictional Frictional Pressure Drop Multipliers at 600 PSIA

(43-024-941)

to interpret the local void fractions in a manner equivalent to that for the 16 pin results. The over-all integrated void fractions appear to be in reasonable agreement with the 16 pin data.

10.0 RECOMMENDATIONS FOR FUTURE STUDIES

1. It is suggested that future research and development programs concerned with pressure losses under similar circumstances utilize low pressure, cold water experiments with prototype geometry and high pressure boiling experiments with scaled-down geometry.
2. The vapor distribution in a boiling rod array offers some interesting challenges, particularly with respect to nuclear reactor applications, which can be satisfactorily met only by continued research and development.

11.0 APPLICATION OF RESULTS TO PATHFINDER

In general the results from the test program reported herein have confirmed the calculational techniques selected earlier, and thus have not necessitated any analysis revisions.

The hydraulic analysis of the boiler core was first presented in (25). A revised analysis, based upon latest design parameters and including the results from the test program has been completed. The results of the later analysis are summarized in Figure 32. The reference nominal recirculation flow is now 66,100 gpm instead of the 64,300 gpm reported in (25).

The complete thermal and hydraulic design and performance analyses (including flow distribution, burnout margin, etc.) based on the test program results is reported in (26).

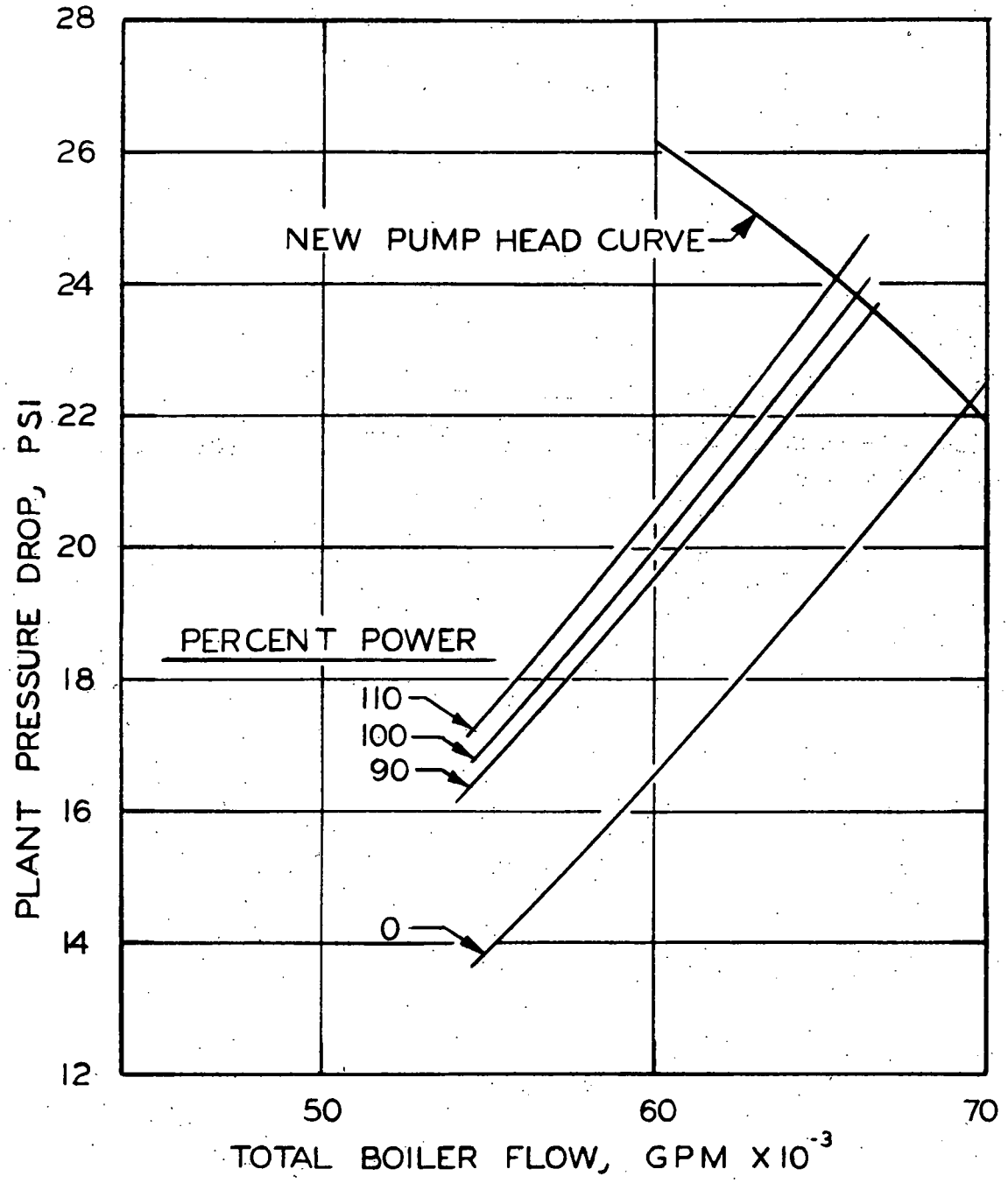

Figure 32 - Pressure Drop-Flow Curves for Various Boiler Powers (43-025-240)

REFERENCES

1. LeTourneau, B. W., R. E. Grimble, and J. E. Zerbe, Trans. Am. Soc. Mech. Engrgs., 79, (1957).
2. Deissler, R. G., and M. F. Taylor, "Analysis of Axial Turbulent Flow and Heat Transfer Through Banks of Rods or Tubes, TID 7529, Reactor Heat Transfer Conference, Pt. I, Book I, 416 - 461.
3. Moody, L. F., Trans. Am. Soc. Mech. Engrs., 66, 671, (1944).
4. LeTourneau, B. W., and R. E. Grimble, "Pressure Drop Tests; Parallel Rod Subassemblies with Various End Connections", WAPD-TH-19, (1955).
5. Martinelli, R. C., and D. B. Nelson, Trans. Am. Soc. Mech. Engrs., 70, 695, (1948).
6. Isbin, H. S., et al, Chem. Eng. Prog. Symposium Series No. 23, Nuclear Engineering - Part VI, 55, 75, (1959).
7. Sher, N. C., and S. J. Green, Chem. Eng. Prog. Symposium Series, Nuclear Engineering - Part VI, 50, 61, (1959).
8. Lottes, P. A., et al, "Experimental Studies of Natural Circulation Boiling and Their Application of Boiling Reactor Performance", Presented at ICPUAE, Geneva, (1958).
9. Lottes, P. A., et al, "Lecture Notes on Heat Extraction From Boiling Water Power Reactors", ANL-6063, (1959).
10. Lottes, P. A., Nuc. Sci. Eng., 9, No. 1, 26, (1961).
11. Maurer, G. W. and A. Weiss, "Results of Vertical Upflow Pressure Drop Tests with Water at 2000 psia for Parallel Flow Through Heated Rod Bundles", WAPD-TH-437, (1958).

12. Janssen, E. and J. A. Kervinen, "Pressure Drop Along a Fuel Cycle Fuel Assembly Various Orifice Configurations", GEAP 3655 (1961).

13. Isbin, H. S., et al, A. I. Ch. E. Jr., 3, 427, (1959).

14. Meyer, J. E., et al, "ART - A Program for the Treatment of Reactor Thermal Transients on the IBM-704", WAPD-TH-156, (1959).

15. Owens, W. L. and V. E. Schrock, "Local Pressure Gradients for Subcooled Boiling Water in Vertical Tubes", ASME Paper 60-WA-249.

16. Frank, S., J. Jicha, and M. Norin, "Local Boiling Heat Transfer Tests", MND-M-1857 (1961).

17. Sher, N. C., "Review of Martinelli-Nelson Pressure Drop Correlation", WAPD-TH-219 (July, 1956).

18. Kemp, R. F., "Kinetic Studies of Heterogeneous Water Reactors", RWD-RL-167, (1959).

19. Hooker, H. H. and G. F. Popper, "A Gamma-Ray Attenuation Method for Void Fraction Determination in Experimental Boiling Heat Transfer Test Facilities", ANL-5766, (1958).

20. Richardson, B. L., "Some Problems in Horizontal Two-Phase Two-Component Flow", ANL-5949, (1959).

21. Petrick, M., "Two-Phase Air-Water Flow Phenomena", ANL-5787, (1958).

22. Condon, R. A. and N. C. Sher, Trans. of ANS Vol. 4, No. 2, (Nov., 1961).

23. Lockhart, R. W. and R. C. Martinelli, Chem. Eng. Prog. 45, 39 - 46 (1949).

24. Jens, W. H. and P. A. Lottes, "Analysis of Heat Transfer, Burnout, Pressure Drop and Density Data for High Pressure Water", ANL-4627, (May, 1951).

25. Sher, N. C., "Hydraulic Analysis of Pathfinder Boiler", ACNP-6104, (Feb., 1961).

26. Bezella, W., et al, "Thermal and Hydraulic Analysis, etc.), ACNP-62017, (Aug., 1962).